Spiking input-output relation for general biophysical neuron models

Daniel Soudry and Ron Meir
Department of Electrical Engineering
The Laboratory for Network Biology Research
Technion, Haifa , Israel

June 14, 2022

*Correspondence: Daniel.Soudry@gmail.com

Abstract

Cortical neurons include many sub-cellular processes, operating at multiple timescales, which may affect their response to stimulation through non-linear and stochastic interaction with ion channels and ionic concentrations. Since new processes are constantly being discovered, biophysical neuron models increasingly become "too complex to be useful" yet "too simple to be realistic". A fundamental open question in theoretical neuroscience pertains to how this deadlock may be resolved. In order to tackle this problem, we first define the notion of a "excitable neuron model". Then we analytically derive the input-output relation of such neuronal models, relating input spike trains to output spikes based on known biophysical properties. Thus we obtain closed-form expressions for the mean firing rates, all second order statistics (input-state-output correlation and spectra) and construct optimal linear estimators for the neuronal response and internal state. These results are guaranteed to hold, given a few generic assumptions, for *any* stochastic biophysical neuron model (with an arbitrary number of slow kinetic processes) under general sparse stimulation. This solution suggests that the common simplifying approach that ignores much of the complexity of the neuron might actually be unnecessary and even deleterious in some cases. Specifically, the stochasticity of ion channels and the temporal sparseness of inputs is exactly what rendered our analysis tractable, allowing us to incorporate slow kinetics.

When aiming to describe a complex system mathematically, it is important to use models that are both simple enough to understand yet complex enough to describe reality at a required level of detail. This tradeoff seems to be ubiquitous in quantitative biology in general [43], and in neuroscience in particular [22]. Since the seminal work of Hodgkin and Huxley [26] on the squid's giant axon, biophysical models of neurons have become an established framework, through which many experimental results can be contrasted, reconciled, interpreted and related to functionality (e.g., [12] and references therein). Such models, called

"Conductance Based Models" (CBMs), are commonly used to investigate intra-cellular dynamics (e.g., dendritic integration [56], axonal propagation [38] and ionic currents [51]) and their relation to neuronal firing patterns [50, 35].

However, CBMs are less popular when modeling networks of neurons [9, 21, 30, 29, 13] or even when attempting to accurately predict the response of a single neuron to stimuli [22]. The main reason for this is that CBMs are complex non-linear models, containing many variables and unknown parameters (sometimes ranging in the hundreds [31, 53]), not all of which can be identified [27]. Moreover, the model response is sometimes highly sensitive to values of these parameters. These issues usually makes CBMs notoriously difficult to tune [22], highly susceptible to over-fitting [12], computationally expensive [41], mathematically intractable [22] and generally "hard to understand" - in the sense that given a specific stimulation pattern and parameter values, it is hard to quantitatively describe the neuronal response of the CBM. Therefore, modelers often prefer to use simplified, phenomenological or statistical, versions of CBMs [32, 16, 5, 47, 28, 4, 55, 40], thereby reducing the biophysical interpretability of the model. Moreover, it is not clear when such approaches neglect essential biophysical constraints or overly simplify the neural response so that it looses some important functional attributes.

To make matters worse, it now seems that even very detailed CBMs should be strictly considered as highly simplified models. For example, most CBMs tend to ignore the stochastic nature of ion channels [45, 25], which was shown to affect the neuronal response and functionality ([14, 60] and references therein). Additionally, it is usually assumed that the synaptic inputs to cortical neurons are rather homogeneous, so that the neuronal firing is dominated by the summation of many such inputs, leading to a simplified analysis (but see [15]). However, recent studies have shown that the distribution of synaptic efficacies in the cortex is log-normal [34], which indicates that the neuronal firing patterns might in fact be dominated by temporally sparse inputs from a small number of strong synapses. Such possibility is supported by the fact that stimulation of a single cortical cell can elicit whisker movements in rats[3]. Finally, new sub-cellular kinetic processes are being discovered at an explosive rate [2, 58, 10]. This variety is particularly large for slow kinetic processes [37], and may affect the neuronal response, as indicated in a recent experiment [20]. Based on these observations, it would be natural to believe that incorporating all of the above complications into the CBM formalism, would lead to intractable and unwieldy equations.

Surprisingly, as we show here, the opposite is the case: when sparse inputs are used in stochastic versions of CBMs, they can become significantly *more* tractable, independently of the number and complexity of the slow kinetic processes added. Specifically, under a "timescale separation" assumption, the temporal response of a general stochastic CBM under sparse stimulation can be accurately and transparently described using an "excitability map", with a significantly smaller number of parameters. These parameters are directly derived from the original CBM, and maintain a well-defined biophysical interpretation. Using this map, simulation time can be dramatically reduced. Furthermore, under stationary input, and an "excitability fixed point" assumption, we can linearize the map and write explicit mathematical expressions for the neuronal input-output relation. Specifically, we find that the mean firing rate can be written as a function of the mean stimulation rate, while the fluctuations can be described using a stochastic dynamical linear system (Fig. 1.1). This

linear system yields a highly interpretable biophysical description of the quantitative dynamics (Fig. 1.1, *bottom*), which contains a feedback loop, similarly to many other biological systems (e.g., [19]). This linear description allows us to use the well established engineering mathematical toolbox to analyze the system, write explicit expressions for the second-order statistics of the neuron (all input-state-output correlations and spectra) and develop linear optimal estimators for the neuronal state and output.

What are the practical implications of our results? In [60] and more recent unpublished work we demonstrate the applicability of our approach to the experimental data of [20], where synaptically isolated individual neurons (from rat cortical culture) were stimulated with physiologically sparse inputs for extended durations of days. Interestingly, the neurons responded in a complex and irregular manner ("$1/f$ spectrum") over the entire range of experimental timescales - from seconds to days. Due to the large number of processes involved at such timescales, many of them unknown or lacking known parameters, this phenomenon cannot be modeled using a purely simulation-based approach. However, using the analytic tools developed here we can circumvent this problem, exactly characterize the classes of CBMs that can generate the observed behavior (given our assumptions), and perform parameter estimation from the observed neuronal response. A further implication is that our methods may provide, in some cases, a definitive characterization of the effects of variability [36] and co-variability [54] of neuronal parameters on its response, since we have closed-form expressions relating response to biophysical parameters. Last, but not least, the methods described here could be also used to significantly improve simulation, analysis and design of CBM-based networks, while allowing CBMs' complexity to increase according to experimental findings.

The remainder of the paper is organized as follows. We begin in section 1 by presenting the general mathematical setup of an abstract neuron under temporally sparse stimulation (section 1.1) and define formally the general class of CBMs (section 1.2). Then, in section 2 we show how to reduce such systems to simple discrete time stochastic maps (section 2.1); derive simple, yet precise, input/output relations for the neuron at the level of spike trains (section 2.2); derive input-output-state 2^{nd} order statistics (section 2.3); explain how to perform linear-optimal estimation of internal neuronal variables (section 2.4) and predict firing patterns; lastly, we demonstrate our results numerically for a specific biophysical model (section 2.5). Recall, however, that our main purpose here was to derive very general results - which are valid for a broad class of biophysically realistic conductance based models. These results are summarized and set in context in section 3. A mathematical appendix delves deeper into the mathematical derivations and expands on some of the numerical issues involved.

1 Methods

1.1 General formalism

Problem definition Isolated cortical neurons are excitable elements that can generate, if stimulated, an Action Potential (AP) response - a "spike" in the cell's membrane voltage. Formally, the "AP event" is defined by a some specific condition. For example: "an AP has occurred if V, the voltage at the axon hillock, has crossed upwards some threshold (say, -10mV)". As seen experimentally [20], APs are not generated spontaneously by cortical

neurons if no stimulation is given (either synaptically or directly) . Therefore, we assume that this is the case (i.e., we do not consider oscillatory neurons). Additionally, in this work we consider short temporally sparse stimulation events. These stimulations can represent either stimulation by direct current pulses (as in [20]), single pre-synaptic APs, or simultaneously occurring groups of pre-synaptic APs. We are interested in finding the "spiking" input-output relation for these neurons under sequences of such stimulation events.

Formally, suppose that at times $\{t_m\}_{m=0}^{\infty}$ a neuron receives a sequence train of *identical* stimuli. We denote by $\{Y_m\}_{m=0}^{\infty}$ the occurrence events of APs at times $\{t_m\}_{m=0}^{\infty}$, i.e., after each stimulation time t_m (Fig. 1.1A)

$$Y_m \triangleq \begin{cases} 1 & , \text{ if an AP occurs} \\ 0 & , \text{ otherwise} \end{cases} . \tag{1.1}$$

Defining $T_m \triangleq t_{m+1} - t_m$, the inter-stimulus interval, and τ_{AP} as the upper timescale of an AP event (Fig. 1.1B) we assume that

1. The neuron does not spontaneously fire APs.
2. The spike times $\{t_m\}_{m=0}^{\infty}$ are temporally sparse, i.e. $\tau_{\text{AP}} \ll T_m$ for every m (a "no collisions" principle).

Objective: Mathematically characterize the relation between $\{Y_m\}$ and $\{T_m\}$ under the most general conditions.

Probabilistic approach Since the specific details of internal neuronal dynamics are not fully understood, we will attempt to answer this question with as few assumptions as possible, in order to maintain a high level of generality. We begin with a rather abstract neuronal model, in which $\mathbf{x}(t)$ is a vector representing the internal neuronal "state" at time t. For example, in the context of the Hodgkin-Huxley model [26] $\mathbf{x}(t)$ represents the voltage, the sodium channel variables and the potassium channel variable. We define $\mathbf{x}_m \triangleq \mathbf{x}(t_m)$ and the history set $\mathcal{H}_m \triangleq \{\{\mathbf{x}_k\}_{k=0}^{m}, \{T_k\}_{k=0}^{m}, \{Y_k\}_{k=0}^{m}\}$ (note that $\mathcal{H}_m \subset \mathcal{H}_{m+1}$). Assuming that $\mathbf{x}_m$ is a "state vector" implies the *Markov property*, namely it is a sufficient statistic on the history to determine the probability of generating an AP at each stimulation,

$$p_{\text{AP}}(\mathbf{x}_m) \triangleq p(Y_m = 1|\mathbf{x}_m) = P(Y_m = 1|\mathbf{x}_m, \mathcal{H}_{m-1}) , \tag{1.2}$$

and, together with Y_m and T_m, its own dynamics

$$P(\mathbf{x}_{m+1}|\mathbf{x}_m, T_m, Y_m) = P(\mathbf{x}_{m+1}|\mathcal{H}_m) , \tag{1.3}$$

which implies causality relations as shown in figure 1.1C under "general models". This causality structure is reminiscent of the well known Hidden Markov Model [52], except that in the present case the output Y_m, affects the transition probability, and we have input T_m.

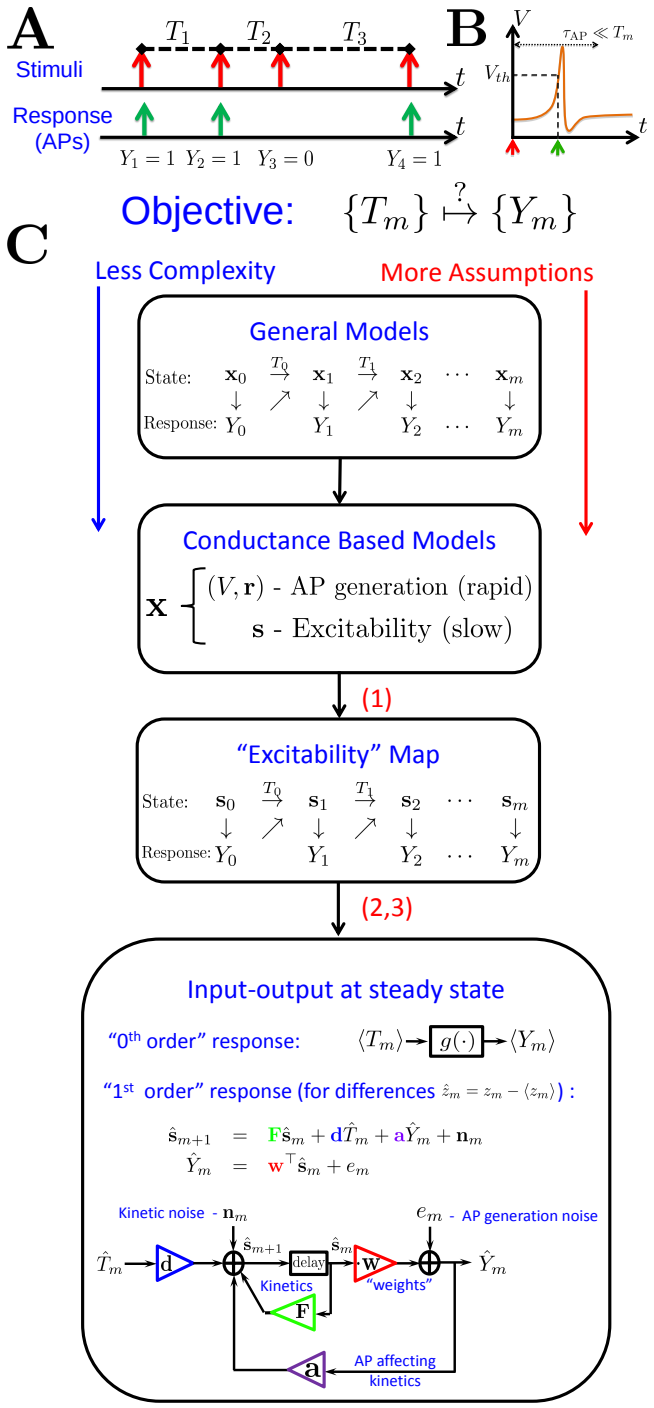

Figure 1.1: **Mathematical analysis - schematic summary:** **A** Main objective - find the inter-stimulus intervals (T_m) to AP occurrences (Y_m) input output relation - for any biophysical neuron model. **B** AP is said to occurred if the voltage V crossed a threshold V_{th} after the stimulus. We examine a "sparse" stimulation regime in which $T_m \gg \tau_{\text{AP}}$, the timescale of AP generation (so stimulation pulses do not "collide"). **C** Model reduction scheme. Each number references the relevant (sufficient) assumptions in text. The end result is the conversion of a complex biophysical neuron model to a simple linear model, with parameters $(\mathbf{F}, \mathbf{d}, \mathbf{a}...)$ directly linked to the biophysical parameters.

Theoretically, if we knew the distributions in 1.2 and 1.3, as well as the initial condition $P(\mathbf{x}_0)$, we could find an exact probabilistic I/O relation

$$P\left(\{Y_k\}_{k=0}^m \,|\, \{T_k\}_{k=0}^m\right) = \int d\mathbf{x}_0 P(\mathbf{x}_0)\, P(Y_0|\mathbf{x}_0) \prod_{k=1}^{m} \int P(Y_m|\mathbf{x}_k)\, P(\mathbf{x}_k|\mathbf{x}_{k-1}, T_{k-1}, Y_{k-1})\, d\mathbf{x}_k \,. \tag{1.4}$$

However, it may be hard to find an expression for $P(\mathbf{x}_k|\mathbf{x}_{k-1}, T_{k-1}, Y_{k-1})$ in general biophysical models, and the computation of 1.4 might be intractable . We therefore propose an alternative approach in the next section.

Stochastic map approach We construct a dynamic "state-space" system with T_m, the inter-stimulus interval lengths, serving as inputs, $\mathbf{x}_m$ representing the neuronal state, and Y_m the output. The model will be augmented with two noise sources. The first noise source is the "innovation part" [1] of the AP generation process,

$$e_m \triangleq Y_m - \langle Y_m|\mathbf{x}_m, \mathcal{H}_{m-1}\rangle = Y_m - p_{\mathrm{AP}}(\mathbf{x}_m) \,, \tag{1.5}$$

where $\langle X|Y\rangle$ is the conditional mean of X given Y. The second noise source is the innovation part for the state increments $\Delta\mathbf{x}_m \triangleq \mathbf{x}_{m+1} - \mathbf{x}_m$

$$\mathbf{n}_m \triangleq \Delta\mathbf{x}_m - \langle \Delta\mathbf{x}_m|\mathbf{x}_m, T_m, Y_m\rangle \,. \tag{1.6}$$

Interestingly, we prove in section A that e_m and $\mathbf{n}_m$ are uncorrelated white noise processes - i.e. $\langle e_m\rangle = 0$, $\langle \mathbf{n}_m\rangle = \langle e_n\mathbf{n}_m\rangle = \mathbf{0}$ and $\left\langle \mathbf{n}_m\mathbf{n}_n^\top\right\rangle = \left\langle \mathbf{n}_m\mathbf{n}_m^\top\right\rangle \delta_{mn}$, $\langle e_m e_n\rangle = \langle e_m^2\rangle\, \delta_{mn}$. Now, defining $\mathbf{h}^+(\mathbf{x}_m, T_m) \triangleq \langle \Delta\mathbf{x}_m|\mathbf{x}_m, T_m, Y_m = 1\rangle$ and $\mathbf{h}^-(\mathbf{x}_m, T_m) \triangleq \langle \Delta\mathbf{x}_m|\mathbf{x}_m, T_m, Y_m = 0\rangle$ and using Eqs. 1.5 and 1.6 it is straightforward to obtain the following non-linear, stochastic, dynamical system

$$\begin{aligned} \mathbf{x}_{m+1} &= \mathbf{x}_m + Y_m\mathbf{h}^+(\mathbf{x}_m, T_m) + (1 - Y_m)\,\mathbf{h}^-(\mathbf{x}_m, T_m) + \mathbf{n}_m \,, & (1.7)\\ Y_m &= p_{\mathrm{AP}}(\mathbf{x}_m) + e_m \,. & (1.8) \end{aligned}$$

Formally, such a system could be used to simulate the neuronal response. Note that in such a simulation, $p_{\mathrm{AP}}(\cdot)$ and $\mathbf{h}^\pm(\cdot,\cdot)$ are deterministic functions while $\mathbf{n}_m$ and e_m are random processes conditioned on $(\mathbf{x}_m, Y_m, T_m)$ and $\mathbf{x}_m$, respectively. In general, in order to perform this simulation, we need to know $p_{\mathrm{AP}}(\cdot)$, $\mathbf{h}^\pm(\cdot,\cdot)$ and the full distribution of $\mathbf{n}_m$ given $(\mathbf{x}_m, Y_m, T_m)$. Although both approaches (Eq. 1.4 and Eqs. 1.7-1.8) are formally equivalent, the latter approach can be more useful in some cases, as we shall later see. For concreteness we examine the canonical class of biophysical neuron models - Conductance-Based models (CBM).

1.2 Stochastic conductance-based models - background

Due to our objective, we are currently not interested in modeling how stimulations from different neurons are integrated in the dendrites or how the propagation in the axon affect the latency of the AP. Therefore, in order simplify the following definitions and analysis, we avoid

unnecessary generality, and consider only models with a single (isopotential) compartment. In a general stochastic CBM for such a point neuron the voltage dynamics is determined by ion channels - protein pores that open and close stochastically in a voltage dependent way [25]. To formalize this, the dynamics of each channel is described as an irreducible continuous time Markov process ([7]), with voltage dependent rates. Given the voltage, all channels are assumed to be independent. Such a mathematical framework is also able, in many cases, to include other cellular processes affecting excitability (e.g., changes in ionic concentrations). However, for descriptive simplicity, we will refer to these Markov processes as "ion channels" only. We index by c the different types channels, $c = 1, ..., C$. For each channel type c there exist $N^{(c)}$ channels, where each channel of type c possesses $K^{(c)}$ internal states. Also, the kinetic transition rate from state j to state i is given by $A_{ij}^{(c)}$. And so, for each channel of type c that resides in state i, the probability that the channel will be in state j after time dt is given by

$$P_{ij}^{(c)} = \begin{cases} A_{ij}^{(c)} dt & , \text{ if } i \neq j \\ 1 - \sum_{j \neq i} A_{ji}^{(c)} dt & , \text{ if } i = j \end{cases} , \tag{1.9}$$

where $\left\{ A_{ij}^{(c)} \right\}$ are generally voltage dependent.

We define $x_k^{(c)}$ to be the fraction of c-type channels in state k, $\mathbf{x}^{(c)}$ to be a column vector composed of $x_k^{(c)}$, $c = 1, 2, \ldots, C$, and $\mathbf{x}$ to be the vector formed by concatenating the $\mathbf{x}^{(c)}$ vectors. The dynamics of the voltage V is then determined by V, $\mathbf{x}$ and $I(t)$, the external current stimulation,

$$\dot{V} = f\left(V, \mathbf{x}, I(t)\right) , \tag{1.10}$$

for an appropriate function f. Note that the neuronal state is now $(V, \mathbf{x})$, and not $\mathbf{x}$ as in section 1.1. For an excitable point neuron model, rather than some general dynamical system, both f and $\left\{ A_{ij}^{(c)} \right\}$ must have adhere to additional constraints.

The excitability constraint

What is an "excitable neuron"? The answer to this question must be formalized mathematically before any generic analytical results can be derived regarding such elements. The main characteristic of the classic HH model [26] is the almost binary "all-or-none" "short-duration" response of its variables to pulse stimulation. It is desirable that an "excitable element" will also have this "all-or-none" "short" response. However, if, as in later models, some of the parameters of the model are changed into slow variables (e.g., slow sodium inactivation [6]), then the response of these variables is neither "all-or-none" nor "short". Can we extend the definition of "excitable" to such cases?

To be able to do this, we need to assume that we can express $\mathbf{x}$ as a combination of a "rapid" component $\mathbf{r}$, which generates the shape of the AP (together with V), and a "slow" component $\mathbf{s}$, which modulates the system over larger timescales. Note that both $\mathbf{r}$ and $\mathbf{s}$ are vectors, comprising multiple components. For example, if only rapid or slow channel types exist, then $\mathbf{x}$ is simply the concatenation of $\mathbf{r}$ and $\mathbf{s}$. For simplicity of notation, we shall henceforth assume that this is the case. However, such a decomposition is readily extendable to cases where some channel types possess both slow and fast kinetics (as we later demonstrate in

the coupled HHS model, in Fig. F.2A; see also [65]). And so, if τ_{AP} and $\tau_{\mathbf{s}}$ are the respective kinetic timescales of $(V, \mathbf{r})$ and $\mathbf{s}$, then $\tau_{\text{AP}} < \tau_{\mathbf{s}}$. Using this decomposition, suppose we "freeze" the dynamics of $\mathbf{s}$ (so that effectively $\tau_{\mathbf{s}}{=}\infty$) and allow only V and $\mathbf{r}$ to evolve in time. We can say the original model describes an "excitable point neuron", if the following conditions hold in the "semi-frozen" model:

1. If $I(t) = 0$, then for all initial conditions, V and $\mathbf{r}$ rapidly (within timescale τ_{AP}) relax to a constant and unique steady state ("rest").

2. Assume that V and $\mathbf{r}$ are near rest, and a short stimulation pulse is given, with amplitude I_0. For certain initial conditions and values of I_0, we get either a stereotypical "strong" response ("AP response") or a stereotypical "weak" response in V ("no AP response"). Only for a very small set of initial conditions and values of I_0, do we get an "intermediate" response ("weak AP response"). By "stereotypical" we mean that the shape of response does not change much between trials or for different initial conditions in $(V, \mathbf{r})$ (however, it can change with $\mathbf{s}$).

Stochastic differential equations form The state vector $\mathbf{x}$ from section 1.1 was split in section 1.2 into three sets of variables: V (voltage), $\mathbf{r}$ (rapid kinetic variables) and $\mathbf{s}$ (slow kinetic variables). The variables V and $\mathbf{r}$ determine AP generation, and so are characterized by the upper timescale of $\boldsymbol{\tau}_{\text{AP}}$. The "excitability" variable $\mathbf{s}$ modulates the AP generation process and operates at a lower timescale of $\boldsymbol{\tau}_{\mathbf{s}}$. In section B we show that we can write an alternative description for this model using the following stochastic differential equations

$$\begin{aligned}
\dot{V} &= f(V, \mathbf{r}, \mathbf{s}, I(t)) && (1.11)\\
\dot{\mathbf{r}} &= \mathbf{A}'(V)\mathbf{r} - \mathbf{b}'(V) + \mathbf{B}'(V, \mathbf{r})\boldsymbol{\xi}' && (1.12)\\
\dot{\mathbf{s}} &= \mathbf{A}(V)\mathbf{s} - \mathbf{b}(V) + \mathbf{B}(V, \mathbf{s})\boldsymbol{\xi} && (1.13)
\end{aligned}$$

where f is some function, $\boldsymbol{\xi}$ and $\boldsymbol{\xi}'$ are vectors of independent white noise processes with zero mean and unit variance, $\mathbf{A}, \mathbf{A}', \mathbf{B}, \mathbf{B}', \mathbf{b}$ and $\mathbf{b}$ are given explicitly as functions of the microscopic voltage-dependent kinetic rates $A_{ij}^{(c)}$, and $\mathbf{B}, \mathbf{B}'$ also depend on $\mathbf{s}$, $\mathbf{r}$ and the numbers of channels $N^{(c)}$, defined in section 1.2. Note both $\mathbf{A}$ and $\mathbf{A}'$ are stable matrices and $\mathbf{D} \triangleq \mathbf{B}\mathbf{B}^{\top}$ and $\mathbf{D}' \triangleq \mathbf{B}'\mathbf{B}'^{\top}$ are both positive definite. Therefore, if V is held constant, the (ensemble) means $\langle \mathbf{s} \rangle$ and $\langle \mathbf{r} \rangle$ tend to $\mathbf{s}_\infty = \mathbf{A}^{-1}\mathbf{b}$ and $\mathbf{r}_\infty = (\mathbf{A}')^{-1}\mathbf{b}'$, respectively. Note that the linear nature of Eq. 1.12-1.13 stems from the fact that ion channels are assumed to be independent given the voltage. Also, the fact that these equations are not directly coupled is not essential (section B) and is made only for mathematical convenience (our results hold for the coupled case, as can be seen in Fig. F.2A).

2 Results

2.1 The excitability map

Given a sequence $\{t_m\}_{m=0}^{\infty}$ of stimulations (as defined in section 1.1), we would like to find explicitly how $V_m = V(t_m)$, $\mathbf{r}_m = \mathbf{r}(t_m)$ and $\mathbf{s}_m \triangleq \mathbf{s}(t_m)$ in a CBM (section 1.2) evolve in time, as in Eq. 1.7 (with $\mathbf{x}_m = (V_m; \mathbf{r}_m; \mathbf{s}_m)$). Theoretically, this could be done by a direct integration of the CBM equations (1.11-1.13) between stimulations. However, such integration does not generally admit an interpretable closed form expression. To overcome this, we will need to assume that the slow kinetics are significantly slower than the inter-stimulus intervals

Assumption 1: $T_m \ll \tau_{\mathbf{s}}$ for every m.

Given this assumption, together with our assumption on the stimulus ($\tau_{\mathrm{AP}} \ll T_m$ for every m, with τ_{AP} possibly extended so to include the timescale of $\mathbf{r}$), and the excitable nature of the CBM, renders the dynamics (1.11-1.13) between stimulations relatively easy to understand. Specifically, between two consecutive stimulations, the slow variable $\mathbf{s}(t)$, starting from its initial condition at the time of the previous stimulation, changes according to the voltage trace $V(t)$ (which enters through the parameters in Eq. 1.13). At the same time, the fast variables $(V(t), \mathbf{r}(t))$ follow stereotypically either the "AP response" ($Y_m = 1$) or the "no-AP response" ($Y_m = 0$), then equilibrate rapidly to some quasi-stationary distribution $q(V, \mathbf{r}|\mathbf{s})$. Summarizing this mathematically, we obtain the following approximations

$$P(Y_m|\mathbf{s}_m) \approx \int P(Y_m|V_m, \mathbf{r}_m, \mathbf{s}_m)\, q(V_m, \mathbf{r}_m|\mathbf{s}_m)\, dV_m d\mathbf{r}_m\,, \quad (2.1)$$

$$P(V_{m+1}, \mathbf{r}_{m+1}, \mathbf{s}_{m+1}|\mathbf{s}_m, T_m, Y_m) \approx q(V_{m+1}, \mathbf{r}_{m+1}|\mathbf{s}_{m+1})\, P(\mathbf{s}_{m+1}|\mathbf{s}_m, T_m, Y_m)\,. \quad (2.2)$$

Using these equations together with Eqs. 1.2, 1.3, we obtain

$$p_{\mathrm{AP}}(\mathbf{s}_m) \triangleq P(Y_m = 1|\mathbf{s}_m) = P(Y_m = 1|\mathbf{s}_m, \mathcal{H}_{m-1})\,, \quad (2.3)$$

$$P(\mathbf{s}_{m+1}|\mathbf{s}_m, Y_m, T_m) = P(\mathbf{s}_{m+1}|\mathbf{s}_m, Y_m, T_m, \mathcal{H}_{m-1})\,, \quad (2.4)$$

where, slightly abusing notation, we redefined $p_{\mathrm{AP}}(\cdot)$. Therefore, due to our assumptions, the "excitability" vector $\mathbf{s}_m$ can now replace the full state vector $\mathbf{x}_m = (V_m; \mathbf{r}_m; \mathbf{s}_m)$ as the sufficient statistic that retains all relevant the information about the history of previous stimuli. Picturesquely, this gives us a Markov process with the causality structure depicted in figure 1.1C under "general models". Since the function $p_{\mathrm{AP}}(\mathbf{s})$ is not affected by the kinetics of $\mathbf{s}$, it can be found by numerical simulation of a single AP using only Eqs. 1.11-1.12, when $\mathbf{s}$ is held constant (see section C.1).

Next, we aim to find a recursive stochastic map for $\mathbf{s}_m$, similarly to Eq. 1.7. Integrating Eq. 1.13, we obtain

$$\mathbf{s}_{m+1} = \mathbf{s}_m + \int_{t_m}^{t_{m+1}} \left(\mathbf{A}(V(t))\,\mathbf{s}(t) - \mathbf{b}(V(t)) + \mathbf{B}(V(t), \mathbf{s}(t))\,\boldsymbol{\xi}(t)\right) dt \quad (2.5)$$

where $\mathbf{A}, \mathbf{b}, \mathbf{B}$ and $\mathbf{D} = \mathbf{B}\mathbf{B}^\top$ depend on the voltage through the kinetic rates. To calculate this integral, let $\alpha(V(t))$ be some microscopic voltage-dependent kinetic rate (some $A_{ij}^{(c)}$, as defined in section 1.2), and average it between two consecutive stimulation pulses given $Y_m, \mathbf{s}_m$ and T_m. We obtain

$$\begin{aligned}
&\int_{t_m}^{t_{m+1}} \alpha(V(t))\, dt | \mathbf{s}_m, Y_m, T_m \\
= \;& \tau_{\mathrm{AP}} \left(\frac{1}{\tau_{\mathrm{AP}}} \int_{t_m}^{t_m+\tau_{\mathrm{AP}}} \alpha(V(t))\, dt \right) + (T_m - \tau_{\mathrm{AP}}) \left(\frac{1}{T_m - \tau_{\mathrm{AP}}} \int_{t_m+\tau_{\mathrm{AP}}}^{t_{m+1}} \alpha(V(t))\, dt \right) \\
\triangleq \;& (\alpha_+(\mathbf{s}_m) Y_m + \alpha_-(\mathbf{s}_m)(1 - Y_m))\, \tau_{\mathrm{AP}} + (T_m - \tau_{\mathrm{AP}})\, \alpha_0(\mathbf{s}_m)
\end{aligned}$$

where in the last line we defined α_0,α_+ and α_- to represent the average rate at rest, during an AP response and during a no-AP response, receptively. Similarly, we augment $\mathbf{A}, \mathbf{D}, \mathbf{B}$ and $\mathbf{b}$ with $\{0, \pm\}$ subscripts to denote the same quantities, when all the kinetic rates are substituted with their averaged $\{0, \pm\}$ equivalents. Since $\mathbf{A}, \mathbf{D}$ and $\mathbf{b}$ are linear combinations of the kinetic rates (section 1.2), this gives

$$\int_{t_m}^{t_{m+1}} \mathbf{A}(V(t))\, dt | Y_m, \mathbf{s}_m, T_m = (\mathbf{A}_+(\mathbf{s}_m) Y_m + \mathbf{A}_-(\mathbf{s}_m)(1 - Y_m))\, \tau_{\mathrm{AP}} + (T_m - \tau_{\mathrm{AP}})\, \mathbf{A}_0(\mathbf{s}_m)$$

and similarly for $\mathbf{D}$ and $\mathbf{b}$. Using this notation, we can perform the integration in Eq. 2.5 and obtain

$$\mathbf{h}^{\pm}(\mathbf{s}_m, T_m) = \tau_{\mathrm{AP}} (\mathbf{A}_{\pm}(\mathbf{s}_m)\, \mathbf{s}_m - \mathbf{b}_{\pm}(\mathbf{s}_m)) + (T_m - \tau_{\mathrm{AP}}) (\mathbf{A}_0(\mathbf{s}_m)\, \mathbf{s}_m - \mathbf{b}_0(\mathbf{s}_m)) + O\left(\left(T_m \tau_{\mathbf{s}}^{-1} \right)^2 \right).$$

Replacing $\mathbf{x}_m$ with $\mathbf{s}_m$ in Eqs. 1.7 and 1.8, we obtain "the excitability map" for the neuronal dynamics

$$\mathbf{s}_{m+1} = \mathbf{s}_m + Y_m \mathbf{h}^+(\mathbf{s}_m, T_m) + (1 - Y_m)\, \mathbf{h}^-(\mathbf{s}_m, T_m) + \mathbf{n}_m\,, \tag{2.6}$$

$$Y_m = p_{\mathrm{AP}}(\mathbf{s}_m) + e_m\,. \tag{2.7}$$

The distribution of $\mathbf{n}_m$ given $\mathbf{s}_m, T_m, Y_m$ can be well approximated to have a normal distribution if channel numbers are sufficiently high and channel kinetics are not too slow [46], with the following variance

$$\left\langle \mathbf{n}_m \mathbf{n}_m^\top | \mathbf{s}_m, T_m, Y_m \right\rangle = \tau_{\mathrm{AP}} (Y_m \mathbf{D}_+(\mathbf{s}_m) + (1 - Y_m)\, \mathbf{D}_-(\mathbf{s}_m)) + (T_m - \tau_{\mathrm{AP}})\, \mathbf{D}_0(\mathbf{s}_m) + O\left(\left(T_m \tau_{\mathbf{s}}^{-1} \right)^2 / N \right),$$

where $N = \min_c N^{(c)}$ ($N^{(c)}$ is the channel number of the c-type channel, defined in section 1.2). Henceforth we shall neglect any second order corrections, since $T_m \tau_{\mathbf{s}}^{-1} \ll 1$, by assumption 1.

Using Eqs. 2.3, 2.6 and the full distribution of $\mathbf{n}_m$, we can now simulate the neuronal response using a reduced model, more efficiently and concisely (fewer parameters) than the full CBM (Eqs. 1.11-1.13). Note that the reduced model parameters, having been deduced from the CBM itself, still retain a biophysical interpretation. Next, we wish to further simplify this reduced model, in the case of stationary input.

2.2 Input-output relations for a stationary input

We now examine the case where $\{T_m\}$ is a Wide Sense Stationary (WSS) process, with mean T_*, so that the assumptions $\tau_{\text{AP}} \ll T_m \ll \tau_{\mathbf{s}}$ are fulfilled with high probability. Assume the neuron is set with a "WSS initial condition", so that $\{\mathbf{s}_m, Y_m\}$ are also WSS processes (e.g., the initial condition is given at $m = -\infty$). For other initial conditions, we get a transient response, similar to that described in [60]. Since in this case the processes $\{\mathbf{s}_m\}, \{Y_m\}$ are WSS, they have constant means $\langle \mathbf{s}_m \rangle = \mathbf{s}_*$ and $\langle Y_m \rangle = p_*$ and possess power spectral densities.

Linearization near a fixed point In order to study the long term dynamics, we linearize the dynamic equations. To do so denote $\hat{T}_m \triangleq T_m - T_*$, $\hat{Y}_m \triangleq Y_m - p_*$, $\hat{\mathbf{s}}_m \triangleq \mathbf{s}_m - \mathbf{s}_*$,$\mathbf{w} \triangleq \nabla p_{\text{AP}}|_{\mathbf{s}^*}$ and $\mathbf{Q} \triangleq \nabla\nabla p_{\text{AP}}|_{\mathbf{s}^*}$ and explicitly solve the system in Eqs. 2.6 2.7 , given the following assumption.

Assumption 2: $\hat{\mathbf{s}}_m$ is small enough, so that with high probability $|\hat{\mathbf{s}}_m| \ll |\mathbf{s}_*|$ (component-wise) and $\left|\mathbf{w}^\top \hat{\mathbf{s}}_m\right| \gg \left|\hat{\mathbf{s}}_m^\top \mathbf{Q} \hat{\mathbf{s}}_m\right|$.

Given assumption 1, this essentially means that $\mathbf{s}_*$ is a stable fixed point of the system (Eqs. 2.6-2.7), and stochastic fluctuations around it are small, compared to the size of the region $\{\mathbf{s}|p_{\text{AP}}(\mathbf{s}_m) \neq 0, 1\}$ (usually determined by the noise level of the rapid system $(V, \mathbf{r})$, from Eq. C.1). Also note that it is guaranteed that, for the "critical" stimulation parameters (for which $p_* = 0, 1$), the fixed point is stable, at least marginally (section D). Given assumption 2, we can approximate

$$p_{\text{AP}}(\mathbf{s}_m) \approx p_* + \mathbf{w}^\top \hat{\mathbf{s}}_m \,, \tag{2.8}$$

which allows us to linearize Eq. 2.7. This essentially means that the components of $\hat{\mathbf{s}}_m$ determine the neuronal response linearly, with the components of $\mathbf{w}$ serving as the effective weights (related to the relevant conductances in the original CBMs). Next, we wish to linearize Eq. 2.6. In order to simplify the resulting expressions, we make one last assumption.

Assumption 3: The average kinetic rates are insensitive to the value of $\mathbf{s}_m$, namely $|d\alpha_{\pm,0}(\mathbf{s}_m)/d\mathbf{s}_m| \ll \alpha_{\pm,0}(\mathbf{s}_m)$.

Consequently, henceforth we approximate the average kinetics rates as constants, as well as their constructs,

$$\mathbf{A}_{\pm,0} \triangleq \mathbf{A}_{\pm,0}(\mathbf{s}^*) \approx \mathbf{A}_{\pm,0}(\mathbf{s}_m) \,,$$

and similarly for $\mathbf{b}$ and $\mathbf{D}$. This approximation results from the typical sigmoid-like shape of voltage dependent rate functions and seem to approximately hold in all cases we checked (see [60]). However, it is non-essential here, and is made above for mathematical convenience. Using the two latter assumptions, and denoting by $\mathbf{I}$ the identity matrix, $\mathbf{A}_1 \triangleq \mathbf{A}_+ - \mathbf{A}_-$, $\mathbf{A}_* \triangleq ((\mathbf{A}_- - \mathbf{A}_0) + p_* \mathbf{A}_1)\tau_{\text{AP}} T_*^{-1} + \mathbf{A}_0$, and similar notations for $\mathbf{b}$ and $\mathbf{D}$ we obtain

$$\begin{aligned} \hat{\mathbf{s}}_{m+1} &\approx T_*(\mathbf{A}_* \mathbf{s}_* - \mathbf{b}_*) + (\mathbf{I} + T_* \mathbf{A}_*)\hat{\mathbf{s}}_m \\ &+ (\mathbf{A}_0(\mathbf{s}_* + \hat{\mathbf{s}}_m) - \mathbf{b}_0)\hat{T}_m + \tau_{\text{AP}}(\mathbf{A}_1(\mathbf{s}_* + \hat{\mathbf{s}}_m) - \mathbf{b}_1)\hat{Y}_m + \mathbf{n}_m \end{aligned} \tag{2.9}$$

Taking expectations and using Eqs. 2.3 and 1.8, we obtain

$$0 = \langle \mathbf{s}_{m+1} - \mathbf{s}_m \rangle \approx T_* \mathbf{A}_* \mathbf{s}_* - T_* \mathbf{b}_*, \tag{2.10}$$

where in the last line we neglected a second order term $\tau_{\text{AP}} \mathbf{w}^\top \left\langle \hat{\mathbf{s}}_m \hat{\mathbf{s}}_m^\top \right\rangle \mathbf{A}_1$. Therefore $\mathbf{s}_* = \mathbf{A}_*^{-1} \mathbf{b}_*$ and we can find p_* implicitly from $p_* = p_{\text{AP}}(\mathbf{s}_*(p_*))$ for a given T_*. We write the explicit solution of this equation as

$$p_* \triangleq g(T_*) . \tag{2.11}$$

Next, using $|\hat{\mathbf{s}}_m| \ll |\mathbf{s}_*|$, Eq. 2.10 and defining $\mathbf{F} \triangleq \mathbf{I} + T_* \mathbf{A}_*, \mathbf{d} \triangleq \mathbf{A}_0 \mathbf{s}_* - \mathbf{b}_0$ and $\mathbf{a} \triangleq \tau_{\text{AP}} (\mathbf{A}_1 \mathbf{s}_* - \mathbf{b}_1)$ we can, approximate Eq. 2.9 as

$$\hat{\mathbf{s}}_{m+1} = \mathbf{F} \hat{\mathbf{s}}_m + \mathbf{d} \hat{T}_m + \mathbf{a} \hat{Y}_m + \mathbf{n}_m , \tag{2.12}$$

which, together with

$$\hat{Y}_m = \mathbf{w}^\top \hat{\mathbf{s}}_m + e_m , \tag{2.13}$$

yields a simple linear state space representation with $\hat{T}_m$ as the input, $\hat{\mathbf{s}}_m$ as the state, $\hat{Y}_m$ as the output and two uncorrelated white noise sources with variances of

$$\Sigma_{\mathbf{n}} \triangleq \left\langle \mathbf{n}_m \mathbf{n}_m^\top \right\rangle = T_* \mathbf{D}_* , \tag{2.14}$$

$$\sigma_e^2 \triangleq \left\langle e_m^2 \right\rangle \approx p_* - p_*^2 , \tag{2.15}$$

where in the last line we neglected the second order term $\mathbf{w}^\top \left\langle \hat{\mathbf{s}}_m \hat{\mathbf{s}}_m^\top \right\rangle \mathbf{w}$. It is straightforward to verify also that $\left\langle \hat{T}_m \mathbf{n}_m \right\rangle = \mathbf{0}$, $\left\langle \hat{T}_m e_m \right\rangle = 0$.

2.3 Input-output statistics

Eq. 2.11 provides a deterministic memoryless non-linear relation between T_* and p_* - the mean statistics of the input and the output. Moreover, the system described in Eqs. 2.12-2.15 gives a dynamic, linear and stochastic relation between $\hat{T}_m$ and $\hat{Y}_m$. This allows the calculation of all second order statistics in the system, e.g., the auto-covariance $R_{\mathbf{xy}}(k) \triangleq \left\langle \hat{\mathbf{x}}_m \hat{\mathbf{y}}_{m+k}^\top \right\rangle$, or, equivalently, the power spectral densities $S_{\mathbf{xy}}(e^{j\omega}) \triangleq \sum_{k=-\infty}^{\infty} R_{\mathbf{xy}}(k) e^{-j\omega k}$ (also $S_{\mathbf{x}} \triangleq S_{\mathbf{xx}}$). As is standard in the theory of discrete time linear systems [48], a particularly simple description emerges using the z-transform $x(z) \triangleq \sum_{k=-\infty}^{\infty} x_k z^{-k}$. First, we denote the transfer functions $\mathbf{H}_o(z) = (\mathbf{I}z - \mathbf{F})^{-1}$ (Open loop) and $\mathbf{H}_c(z) = \left(\mathbf{I}z - \mathbf{F} - \mathbf{a}\mathbf{w}^\top\right)^{-1}$ (Closed loop), and note that by the Sherman Morrison lemma $\mathbf{w}^\top \mathbf{H}_c(z) = \mathbf{w}^\top \mathbf{H}_o(z) \left(1 - \mathbf{w}^\top \mathbf{H}_o(z) \mathbf{a}\right)^{-1}$. Then, reading off the diagram in bottom of Fig. 1.1C, we obtain

$$\hat{\mathbf{s}}(z) = \mathbf{H}_c(z) \left(\mathbf{n}(z) + \mathbf{d} \hat{T}(z) + \mathbf{a} e(z) \right) , \tag{2.16}$$

$$\hat{Y}(z) = \mathbf{w}^\top \mathbf{H}_c(z) \left(\mathbf{n}(z) + \mathbf{d} \hat{T}(z) + \mathbf{a} e(z) \right) + e(z) . \tag{2.17}$$

Using standard techniques ([48]) we find

$$S_{\mathbf{s}}\left(e^{j\omega}\right) = \mathbf{H}_c\left(e^{j\omega}\right) \left(\mathbf{\Sigma}_{\mathbf{n}} + \mathbf{a}\mathbf{a}^\top \sigma_e^2 + \mathbf{d}\mathbf{d}^\top S_T\left(e^{j\omega}\right) \right) \mathbf{H}_c^\top\left(e^{-j\omega}\right) , \tag{2.18}$$

$$S_{YT}\left(e^{j\omega}\right) = \mathbf{w}^\top \mathbf{H}_c\left(e^{j\omega}\right) \mathbf{d} S_T\left(e^{j\omega}\right) , \tag{2.19}$$

$$S_Y\left(e^{j\omega}\right) = \mathbf{w}^\top \mathbf{H}_c\left(e^{j\omega}\right) \left(\mathbf{\Sigma}_{\mathbf{n}} + \mathbf{d}\mathbf{d}^\top S_T\left(e^{j\omega}\right) \right) \mathbf{H}_c^\top\left(e^{-j\omega}\right) \mathbf{w} + \sigma_e^2 \left| 1 + \mathbf{w}^\top \mathbf{H}_c\left(e^{j\omega}\right) \mathbf{a} \right|^2 . \tag{2.20}$$

For low frequencies it is sometimes more convenient to use the continuous-time versions of the PSDs, $S_X(f) \triangleq T_* S_X(e^{j\omega})_{\omega=2\pi f T_*}$ for $f \ll T_*^{-1}$, which are approximated by

$$\begin{aligned}
S_{\mathbf{s}}(f) &= \left(\mathbf{A}_* + \mathbf{a}\mathbf{w}^\top T_*^{-1} - 2\pi f j\right)^{-1} \left(\mathbf{D}_* + T_*^{-1}\mathbf{a}\mathbf{a}^\top \sigma_e^2 + \mathbf{d}\mathbf{d}^\top S_T(f)\right) \left(\mathbf{A}_* + \mathbf{a}\mathbf{w}^\top T_*^{-1} + 2\pi f j\right)^{-1} && (2.21)\\
S_{YT}(f) &= \mathbf{w}^\top (\mathbf{A}_* - 2\pi f j)^{-1} \mathbf{d} S_T(f) \left(1 - T_*^{-1}\mathbf{w}^\top (2\pi f j - \mathbf{A}_*)^{-1} \mathbf{a}\right)^{-1} && (2.22)\\
S_Y(f) &= \left(\mathbf{w}^\top (\mathbf{A}_* - 2\pi f j)^{-1} \left(\mathbf{D}_* + \mathbf{d}\mathbf{d}^\top S_T(f)\right) \left(\mathbf{A}_*^\top + 2\pi f j\right)^{-1} \mathbf{w} + \sigma_e^2\right) && (2.23)\\
&\cdot \left|1 - T_*^{-1}\mathbf{w}^\top (2\pi f j - \mathbf{A}_*)^{-1} \mathbf{a}\right|^{-2} .
\end{aligned}$$

Note that (assuming no zero-pole cancellations) in Eqs. 2.16-2.23 all the transfer functions and spectra are of order M and have the same poles, which are the eigenvalues of the characteristic polynomial $\left|\lambda \mathbf{I} - \mathbf{F} - \mathbf{a}\mathbf{w}^\top\right| = 0$ in the discrete case, and

$$\left|\lambda \mathbf{I} - \mathbf{A}_* - T_*^{-1}\mathbf{a}\mathbf{w}^\top\right| = 0 \tag{2.24}$$

in the continuous time case. Since we assumed that the fixed point at $\mathbf{s}_*$is stable, necessarily the solutions for these equation must fulfill $|\lambda| < 1$ in the discrete case and $\mathrm{Re}[\lambda] < 0$ in the continuous case, respectively.

2.4 Optimal linear filtering

The system in Eqs. 2.12-2.15 is also useful for obtaining optimal linear estimators of $\hat{Y}_m$ and $\hat{\mathbf{s}}_m$. Using spectral factorization ([1]), we convert the system to the innovation form ([1])

$$\begin{aligned}
\hat{\mathbf{s}}_{m+1} &= \left(\mathbf{F} + \mathbf{a}\mathbf{w}^\top\right) \hat{\mathbf{s}}_m + \mathbf{d}\hat{T}_m + \mathbf{q} v_m\\
\hat{Y}_m &= \mathbf{w}^\top \hat{\mathbf{s}}_m + v_m
\end{aligned}$$

with $\mathbf{q} = \mathbf{a} + \mathbf{F}\mathbf{P}\mathbf{w}\left(\mathbf{w}^\top \mathbf{P}\mathbf{w} + \sigma_e^2\right)^{-1}$, where $\mathbf{P}$ is the solution of

$$\mathbf{P} = \mathbf{F}\mathbf{P}\mathbf{F}^\top - \left(\mathbf{w}^\top \mathbf{P}\mathbf{w} + \sigma_e^2\right)^{-1} \mathbf{F}\mathbf{P}\mathbf{w}\mathbf{w}^\top \mathbf{P}\mathbf{F}^\top + \Sigma_{\mathbf{n}} ,$$

derived from the general discrete-time algebraic Riccati equation, where v_m is a scalar white noise variable with zero mean and variance σ_v^2 , with $\sigma_v^2 = \mathbf{w}^\top \mathbf{P}\mathbf{w} + \sigma_e^2$. This innovation form is directly related to optimal linear filter - the Kalman filter. This is the case since $\mathbf{q}$ is the Kalman gain, while σ_v^2 and $\mathbf{P}$ are equal to the Mean Square Errors (MSEs) of a Kalman filter estimation of $\hat{Y}_m$ and $\hat{\mathbf{s}}_m$, respectively, in the case of zero input [1]. Moreover, the z transform of this system

$$\hat{Y}(z) = H_{\text{signal}}(z) \hat{T}(z) + H_{\text{noise}}(z) v(z) , \tag{2.25}$$

with $H_{\text{signal}}(z) = \mathbf{w}^\top \mathbf{H}_c(z) \mathbf{d}$ and $H_{\text{noise}}(z) = \mathbf{w}^\top \mathbf{H}_c(z) \mathbf{q} + 1$, describes more concisely the contributions of the input and noise to the output as an ARMAx model [33].

2.5 Examples and simulations

Having presented the general formalism in section 1.2 we consider next several concrete examples, and show that they all fall into the general formalism developed. We begin with the HHS model (proposed in [6], see [60] for further details and references, and section E for exact parameters) which augments the classic HH model with an additional slow inactivation process of the sodium conductance. The model includes the uncoupled stochastic Hodgkin-Huxley (HH) model equations ([26, 18])

$$\begin{aligned} C\dot{V} &= \bar{g}_{Na} s m^3 h \left(E_{Na} - V\right) + \bar{g}_K n^4 \left(E_K - V\right) + \bar{g}_L \left(E_L - V\right) + I\left(t\right) && (2.26) \\ \dot{r} &= \alpha_r\left(V\right)\left(1-r\right) - \beta_r\left(V\right) r + \sigma_r\left(V,r\right)\xi_r, \text{ for } r = m,n,h && (2.27) \end{aligned}$$

with the additional kinetic equation for slow sodium inactivation

$$\dot{s} = \delta\left(V\right)\left(1-s\right) - \gamma\left(V\right) s + \sigma_s\left(V,r\right)\xi_s\,, \tag{2.28}$$

where V is the membrane voltage, $I\left(t\right)$ is the input current, m, n and h are ion channel "gating variables", $\alpha_r\left(V\right), \beta_r\left(V\right), \delta\left(V\right)$, and $\gamma\left(V\right)$ are the voltage dependent kinetic rates of these gating variables, C is the membrane's capacitance, E_K, E_{Na} and E_L are ionic reversal potentials, $\bar{g}_K, \bar{g}_{Na}$ and $\bar{g}_L$ are ionic conductances $\sigma_r\left(V,r\right) = \sqrt{N_r^{-1}\left(\alpha_r\left(V\right)\left(1-r\right) + \beta_r\left(V\right) r\right)}$ and $\sigma_s\left(V,s\right) = \sqrt{N_s^{-1}\left(\delta\left(V\right)\left(1-s\right) + \gamma\left(V\right) s\right)}$.

Map parameters Comparing with Eq. 1.13 we find $A\left(V\right) = -\gamma\left(V\right) - \delta\left(V\right)$, $b\left(V\right) = \delta\left(V\right)$, $B\left(V,s\right) = \sigma_s\left(V,s\right)$. Following the reduction technique described in section 2.1, we numerically find the average rates $\gamma_{\pm,0}\left(\mathbf{s}\right)$ and $\delta_{\pm,0}\left(\mathbf{s}\right)$ (as in [60], where we used an $H/M/L$ notation instead of the current notation $+/-/0$ here) τ_{AP} and $p_{\text{AP}}\left(\mathbf{s}\right)$ (section C.1). From Eq. 2.11 we obtain p_*, $\mathbf{w}$ and $\mathbf{s}_*$ for a given T_*. Defining $f_{\text{in}} \triangleq T_*^{-1}$ and $\bar{f}_{\text{out}} \triangleq p_* f_{\text{in}}$ yields a direct relation between stimulation rate and firing rate (Fig 2.1A). The average inactivation rate at steady state is denoted by

$$\gamma_* \triangleq \left(p_*\gamma_+\left(\mathbf{s}_*\right) - \left(1-p_*\right)\gamma_-\left(\mathbf{s}_*\right)\right)\tau_{\text{AP}} T_*^{-1} + \left(1 - \tau_{\text{AP}} T_*^{-1}\right)\gamma_0\left(\mathbf{s}_*\right)\,,$$

and similarly for the recovery rate δ_*. And so, $A_* = -\gamma_* - \delta_*, b_* = -\delta_*$, $s_* = \delta_*/\left(\gamma_* + \delta_*\right)$, $d = \left(\gamma_*\delta_0 - \gamma_0\delta_*\right)/\left(\gamma_* + \delta_*\right)$ and $D_* = N_s^{-1}\left(\delta_*\gamma_*/\left(\gamma_* + \delta_*\right)\right)$. Denoting $\gamma_1 \triangleq \gamma_+\left(s_*\right) - \gamma_-\left(s_*\right)$ and similarly for δ_1, we can also obtain $a = \tau_{\text{AP}}\left(\gamma_*\delta_1 - \gamma_1\delta_*\right)/\left(\gamma_* + \delta_*\right)$.

Power spectral densities Substituting in Eq. 2.20 for example, assuming periodic input T_m gives

$$S_Y\left(f\right) = \frac{w^2\left(D_* + d^2 S_T\left(f\right)\right) + T_*\sigma_e^2\left(\left(2\pi f\right)^2 + A_*^2\right)}{\left(2\pi f\right)^2 + \left(A_* + T_*^{-1} w a\right)^2} \tag{2.29}$$

Note that this is the shape of a high pass filter when $S_T\left(f\right) \equiv 0$ (in which case the input to the system is purely its internal white noise), as can be seen in Fig 2.1B (*top*), where we compare this analytic result with the simulation and the full CBM (2.26,2.27,2.28) and a simulation of the excitability map. Since it follows in this case from (2.25) that $S_Y\left(f\right) = \left|H_{\text{noise}}\left(f\right)\right|^2 \sigma_v^2$, this indicates that $H_{\text{noise}}\left(f\right)$ is also a high pass filter. In contrast, $S_s\left(f\right)$ has the shape of low

pass filter (Fig 2.1B , *bottom*). To examine the limit of our mathematical results, in figure F.2 we compare the analytic and simulated $S_Y(f)$ for other models, as described in section E. Similarly,

$$S_{YT}(f) = \frac{wd}{2\pi f j - \left(A_* + T_*^{-1} wa\right)^2} S_T(f) , \tag{2.30}$$

has the shape of a low pass filter. Since $S_{YT}(f) = H_{\text{signal}}(f) S_T(f)$, this indicates that $H_{\text{signal}}(f)$ is a low pass filter. We compare this result with a simulation of the full CBM (Fig 2.1D) . Since the estimation of the cross-spectrum is known to be noisy ([49] p.321, and see Fig. F.3), we only show a part with a relatively low estimation noise level.

Optimal linear filtering Using the Kalman filter for the HHS model, as derived in section 2.4, we can estimate the internal state $\hat{s}_m$ given $\left\{\{T_k\}_{k=0}^{m-1}, \{Y_k\}_{k=0}^{m-1}\right\}$ quite well, with low MSE (Fig. 2.1C). Also, we tested the Kalman predictor estimate for the spiking event Y_m given $\left\{\{T_k\}_{k=0}^{m-1}, \{Y_k\}_{k=0}^{m-1}\right\}$, at various noise levels. We compared the predictions with the trivial "mean" estimate $Y_m^{\text{est}} = p_*$ (a lower bound on performance), an "oracle" estimate $Y_m^{\text{est}} = p_{\text{AP}}(s_m)$ (an upper bound on performance), and two "black box" models (available in the Matlab system identification toolbox): ARMAx(1,1,1) and a 1st order State Space model (see [33] - other black box models tested performed similarly). We measured the predictors' performance using the error probability $P_{\text{error}} \triangleq P\left(Y_m \neq \mathcal{I}\left(Y_m^{\text{est}} > 1/2\right)\right)$, instead of the MSE, since Y_m is a binary variable; here $\mathcal{I}()$ is the indicator function. As can be seen in Fig. 2.1D, for $N = 10^4$ and $N = 10^6$, all estimators Y_m^{est} perform equally (except for state space model) - poorly yet optimally, since $P_{\text{error}}^{\text{mean}} = P_{\text{error}}^{\text{oracle}}$, which indicates that the AP generation noise level is high. Note however, that $\hat{s}$ can be accurately estimated even in this case (Fig. 2.1C). For $N \geq 10^8$, the noise level decreases, and all estimators show improvement over the mean predictor as N increases. The black box model performances are always close to the oracle bound (and so, perform optimally), while the model based Kalman filter is slightly above this bound at $N = 10^{10}$. This is not surprising since for $N = 10^{10}$ the fixed point s_* looses stability (due to a flip bifurcation) and a limit cycle becomes the new stable attractor (as in the deterministic model [60]), which invalidates assumption 2, and so our linear model can become inaccurate. At $N = 10^{12}$ the dynamics become almost completely deterministic, and so the estimation error goes to zero for all non-trivial predictors - even our possibly inaccurate model.

Since our model for $\hat{s}_m, \hat{Y}_m$ is linear, it is easy for linear black box models to perform accurate system identification. Therefore, it is not surprising that the black box estimators manage to perform well as the model-based Kalman filter. In fact, since that the black-box models remain close to the oracle bound even when our linear model might be inaccurate hints that a different linear model might be derived there. However, the main issue to note is that the black box models cannot estimate accurately the state space structure $(\mathbf{F}, \mathbf{d}, \mathbf{w}, ...)$ or $\hat{s}_m$, unless some information is given on the state-space structure, in which case they become grey-box models. In other words, our dynamic model, given by Eqs. 2.9 and 2.11, allows us to predict the internal state variables and AP sequences as accurately as any predictor, while maintaining a compact and transparent biophysical interpretation.

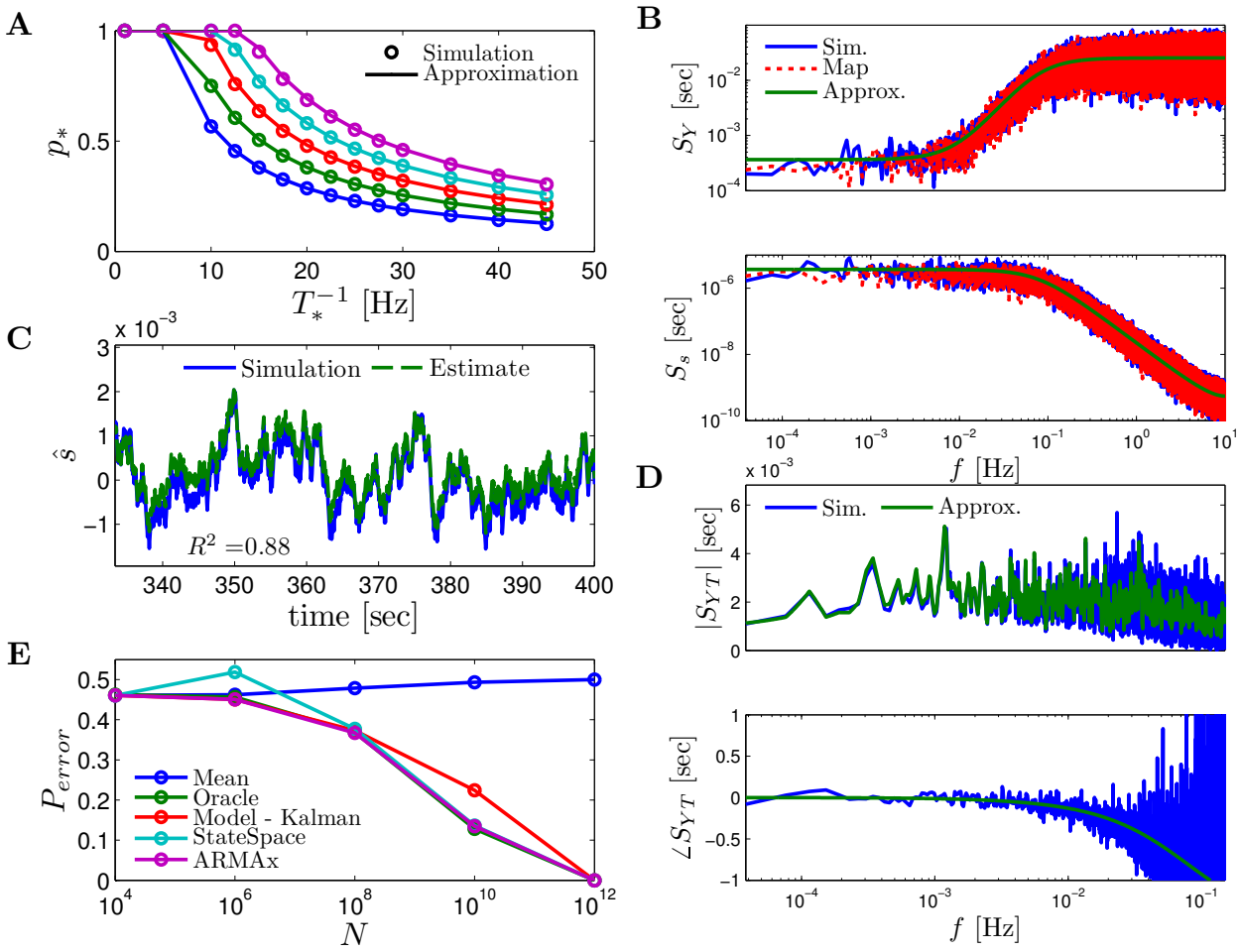

Figure 2.1: **Comparisons of simulation with mathematical results, for stochastic HHS model. A** Eq. 2.11 compared with a simulation of the full CBM (Eqs. 1.11-1.13), for different currents ($I_0 = 7.5, 7.7, 7.9, 8.1, 8.3$ μA from bottom to top). **B** $S_Y(f)$ and $S_s(f)$ at periodical stimulation, compared with a simulation of the full CBM and the excitability map (Eqs. 2.6-2.7). **C** Kalman filter estimation of $\hat{s}$, for same CBM simulation as in B. **D** Amplitude and phase of $S_{YT}(f)$, for Poisson stimulation. Note that frequency range was cut due to spectral estimation noise (see Fig. F.3) **E** Probability of estimation error of Y_m, for various N, and various estimators, as described in section 2.5.

3 Discussion

Any model is "a simplification and an idealization, and consequently a falsification [63]. What details can be 'idealized away' when constructing and using biophysical neuron models? To formalize this issue we must properly define: (1) What constitutes the class of "excitable neuron" models. (2) The relevant questions that models from that class should answer.

Historically, the answer to the first question was essentially "the set of all models generated by electrophysiologists to model neuronal behavior". Such an answer was perhaps satisfying when only a few models of excitable membranes (e.g., the HH model [26]) existed. However, since that time the class of allowable models has significantly expanded and is still growing rapidly with the discovery of new biophysical processes [2, 58, 10]. Therefore, if any generic results are to be derived regarding this set, we must first find a more useful definition. In this work we suggest a general definition for what constitutes an "excitable element" (section 1.2), and, more specifically, the subset of "Conductance Based-Models" (CBMs), which covers most of the models for excitable point neurons usually used in the literature.

The answer to the second question depends on the level of investigation. Commonly, neurons are explored experimentally by injecting current and measuring the membrane voltage. Therefore, relating to experiments, modelers have often tried to use the CBMs to find an Input-Output (I/O) relation from current to voltage. This approach is generally useful since it is "close to the measured data" and can be used to fit biophysical parameters [11], but has two main disadvantages. First, in most cases, due to the complexity of CBMs, it can only be studied using a numerical simulation of the model. However, many parameters are often unknown, and the simulation results can change unexpectedly due to changes in those unknown parameters. Due to the large volume of the parameter space and its complexity (e.g., different I/O relations are given by non-convex parameter sets [36]), it is hard to perform a proper numerical scan of that space. Therefore, in many cases the relevance of such simulation results is not clear. Second, according to the main dogma of neuroscience, neurons communicate using Action Potentials (AP), a.k.a."spikes". Therefore, if we are to use a neuronal model to understand how different neurons interact in a physiological setting, a current to voltage I/O might be less useful, since it is less relevant functionally. And so, to answer the second question, it seems reasonable to require that in a "good neuronal model" we should be able to accurately characterize a "spiking I/O" relating input spikes to output spikes, and to understand how this I/O changes when biophysical parameters are varied. In this work we have found precise conditions on the stimulus and model parameters under which CBM models can be transformed into such "good models", and show how such a transformation can be executed.

Analytical results More concretely, we established a formalism through which any "excitable element" under a sparse stimulation protocol can be analyzed (section 1.1). Applying this formalism to a general stochastic CBM (section 1.2) with arbitrarily complex dynamics, we transformed the continuous time mathematical description into a much simpler "excitability map" (Eqs. 2.6-2.7), which has far fewer parameters, is easily interpretable in functional terms, and is much more efficient in numerical simulations. This transformation is guaranteed to be accurate given a timescale separation assumption (1). For a stationary input, we

used a linear approximation for the steady state map dynamics (Eqs. 2.12-2.13), which is guaranteed to be accurate given assumptions 2 and 3. This allows us to write expressions for the mean firing rate (Eq. 2.11) and all second order statistics (Eqs. 2.18-2.20), and to construct optimal filters for the neuronal response and state (section 2.4).

Numerical results We tested the mathematical expressions numerically (Figs. 2.1, F.1 and F.2) for various parameters and models, and found a good match, even in cases which did not strictly obey our assumptions. For example, we show that our results hold reasonably well even if assumption 1 and 2 do not hold (Fig F.1). Additionally, although we did not consider synapses, in Fig. F.2D, we added to the model a synapse undergoing short term plasticity through synaptic depression (based on [61]), and obtained similar results. Therefore, it should be straightforward to include synaptic dynamics (including STDP) and also passive dendritic tree in the framework. However, including more than a single excitable compartment might be somewhat more involved, since the neuron no longer possesses an "all-or-none" response as assumed here. Instead it can display a partial response, in which some of the compartments spike while others do not (see also [60]).

Further Generalizations Additional extensions, which we did not consider here, are the inclusion of ion-channel interactions at the population level. The existence of such effects in CBMs is currently debatable at the fast timescales ([44] and Brief Communications arising), but are known to exist through different cellular mechanisms that might affect excitability (e.g., gene regulation networks). Such effects might render channel dynamics non-linear ([23, 46]). This might happen if assumptions 1 or 2 become grossly invalid. In both cases, the response of the neuron can be non-linear, and reflect a more "digital" kind of computation (e.g. [8]). However, in some cases, it might still be possible that a linear model can capture well the general model dynamics (Eq. 1.7- Eq. 1.8) near some steady state attractor, if $\hat{T} \ll T_*$ (note that this was not required for linearity in our formalism, given the timescale separation assumption 1).

Estimation The hypothesis relating to the linearity of the residual stochastic process is corroborated by the good performance of linear black-box predictors (Fig. 2.1E) when assumption 2 breaks down. In any case, the relevance of the model suggested here to a realistic neuron, can be directly tested experimentally through the linearity of the neural response (e.g,. by using sinusoidal $\hat{T}_m$). If the neuron responds linearly, then linear black-box predictors (such as ARMAx-based predictors) should perform optimally (no need for the more general Box-Jenkins-based predictor ([33]), as indicated by Eq. 2.25). However, as indicated by Fig. 2.1E, in some cases (e.g., $N = 10^6$), optimal may not be very different from useless due to the high level of stochasticity. Also, even in such cases the neuronal state can be estimated well (Fig. 2.1C). Both facts indicate that the intrinsic AP generation mechanism in the neuron is rather noisy, so simulation of predictors based on deterministic CBMs (e.g., [4]) might be misleading. We perform further investigation of these matters when we use the results describe here to explain the experimental data of [20].

Functionality and Networks The resulting input-output relation we have described here is similar to linear analog circuits working at some operating point $(\mathbf{s}_*, p_*)$, determined by the input bias (T_*). Such a system could be used a an adaptive filter - where the mean firing rate tunes the parameters of the linear filter, and its spike time input-output relation. Note that although the filter is linear when its input is $\hat{T}_m$ and its output is $\hat{Y}_m$, it is not linear when considering the mapping between the input spike train to the output spike train. And so, when embedded in a network, the network is not necessarily linear. In any case, since different input spikes generally do not "collide" in our framework (the $\tau_{\text{AP}} \ll T_m$ assumption)the computations performed by such a filter are inherently different from the standard paradigm of neuronal computation [57], which usually involves the summation of different spikes arriving together. Such a summation may depend on details of millisecond delays between arriving spikes (a rather standard situation [20]), and might be less robust than a stochastic computation based on slow kinetics, as presented here.

Appendix

A Noise correlations

Recall that we defined $e_m \triangleq Y_m - p_{\text{AP}}(\mathbf{x}_m)$. Note that $\langle e_m | \mathcal{H}_{m-1}, \mathbf{x}_m \rangle = \langle e_m | \{\mathbf{x}_k\}_{k=0}^m \rangle = \langle e_m | \mathbf{x}_m \rangle = 0$, and therefore $\langle e_m f(\mathcal{H}_{m-1}, \mathbf{x}_m) \rangle = 0$ for any deterministic function f. Also, from its definition, $e_m = f(\mathcal{H}_m)$ for some deterministic function f, and so, for $n > m$

$$\langle e_n e_m \rangle = \langle \langle e_n e_m | \mathcal{H}_{n-1}, \mathbf{x}_n \rangle \rangle = \langle \langle e_n | \mathcal{H}_{n-1}, \mathbf{x}_n \rangle e_m \rangle = 0\,,$$

and similarly for $m < n$. So e_m is a white noise process with $\langle e_n e_m \rangle = \sigma_e^2 \delta_{mn}$ and $\sigma_e^2 = \langle p_{\text{AP}}(\mathbf{x}_m) \rangle - \langle p_{\text{AP}}^2(\mathbf{x}_m) \rangle$. We defined $\mathbf{n}_m \triangleq \Delta\mathbf{x}_m - \langle \Delta\mathbf{x}_m | \mathbf{x}_m, T_m, Y_m \rangle$. Note that $\langle \mathbf{n}_m | \mathcal{H}_m \rangle = \langle \mathbf{n}_m | \mathbf{x}_m, T_m, Y_m \rangle = 0$ and therefore $\langle \mathbf{n}_m f(\mathcal{H}_m) \rangle = 0$ for any deterministic function f. Note also that from its definition, $\mathbf{n}_m = f(\mathcal{H}_m, \mathbf{x}_{m+1})$ for some deterministic function f. Since $\{\mathcal{H}_m, \mathbf{x}_{m+1}\} \subset \mathcal{H}_{m+k}$ for all $k \geq 1$, we obtain for $n > m$

$$\left\langle \mathbf{n}_n \mathbf{n}_m^\top \right\rangle = \left\langle \left\langle \mathbf{n}_n \mathbf{n}_m^\top | \mathcal{H}_n \right\rangle \right\rangle = \left\langle \langle \mathbf{n}_n | \mathcal{H}_n \rangle \mathbf{n}_m^\top \right\rangle = 0,$$

and similarly for $m < n$. So $\mathbf{n}_m$ is a white noise process, with $\left\langle \mathbf{n}_m \mathbf{n}_m^\top \right\rangle = \Sigma_{\mathbf{n}} \delta_{nm}$. Additionally, we note that $\mathbf{n}_m$ and e_m are uncorrelated

$$\langle e_n \mathbf{n}_m \rangle = \begin{cases} \langle \mathbf{n}_m \langle e_n | \mathcal{H}_{n-1}, \mathbf{x}_n \rangle \rangle & , n > m \\ \langle e_n \langle \mathbf{n}_m | \mathcal{H}_m \rangle \rangle & , n \leq m \end{cases} = 0\,.$$

B Derivation of stochastic differential equations

To facilitate mathematical analysis and efficient numerical simulation, it is sometimes desirable to approximate stochastic CBMs using stochastic differential equations (SDE). This was initially suggested by [18], but their method suffered from several problems ([24]). In a recent

paper ([46]) a more general method was derived, which had none of the previous problems, and was shown numerically to produce a very accurate approximation of the original Markov process description. Here we derive the neuronal SDEs, shown in Eq. 1.12-1.13. Using the stochastic CBM notations with Eqs. 1.9-1.10 and the method described in [46] we obtain the following SDE for the dynamics of $\mathbf{x}^{(c)}$

$$\dot{\mathbf{x}}^{(c)} = \mathbf{A}^{(c)}\mathbf{x}^{(c)} + \mathbf{B}^{(c)}\boldsymbol{\xi}^{(c)}, \tag{B.1}$$

where the elements of the rate matrix $\mathbf{A}^{(c)}$ are defined to be $A_{ij}^{(c)}$ for all $i \neq j$ and $A_{ii}^{(c)} = -\sum_{j\neq i} A_{ji}^{(c)}$ on the diagonal; $\boldsymbol{\xi}^{(c)}$ is a white noise vector process - meaning it has zero mean and auto-covariance $\left\langle \boldsymbol{\xi}^{(c)}(t)\left(\boldsymbol{\xi}^{(c)}(t')\right)^{\top}\right\rangle = \mathbf{I}\delta_{c,c'}\delta(t-t')$ where $\mathbf{I}$ is the identity matrix,$\langle\cdot\rangle$ denotes an ensemble average, $\delta(t)$ is the Dirac delta function, and $\delta_{c,c'} = 1$ if $c = c'$ and 0 otherwise; and $\mathbf{B}^{(c)}$ is defined so that each component of $\boldsymbol{\xi}^{(c)}$ is associated with a transition pair $i \leftrightharpoons j$, multiplied by $\sqrt{\left(A_{ij}^{(c)}x_j^{(c)} + A_{ji}^{(c)}x_i^{(c)}\right)/N^{(c)}}$, and appears in the equation for $\dot{x}_i^{(c)}$ and $\dot{x}_j^{(c)}$ with opposite signs. Note that $\mathbf{B}^{(c)}$ is not necessarily square since it has $K^{(c)}$ rows but the number of columns is equal to the number of transition pairs.

Since $x_k^{(c)}$ denote fractions, $\sum_k x_k^{(c)} = 1$, for all c. We use this constraint, together with the irreducibility of the underlying ion channel process, to reduce by one the dimensionality of B.1. Defining $\mathbf{J}$ to be the $\mathbf{I}$ with it last row removed, $\mathbf{e} = (0,0,...,1)^{\top}$, $\mathbf{u} = (1,1,...,1)^{\top}$, $\mathbf{H} = \left(\mathbf{I} - \mathbf{e}\mathbf{u}^{\top}\right)\mathbf{J}^{\top}$, $\tilde{\mathbf{A}}^{(c)} = \mathbf{J}\mathbf{A}^{(c)}\mathbf{H}$, $\tilde{\mathbf{B}}^{(c)} = \mathbf{J}\mathbf{B}^{(c)}$ (with $x_{K^{(c)}}^{(c)}$ replaced by $1-x_1-x_2...-x_{K^{(c)}-1}$) and $\mathbf{b}^{(c)} \triangleq -\mathbf{J}\mathbf{A}^{(c)}\mathbf{e}$ ($\tilde{\mathbf{A}}^{(c)}$ is invertible), we obtain the following equation for smaller state vector $\mathbf{y}^{(c)} = \mathbf{J}\mathbf{x}^{(c)}$ (which has only $K^{(c)} - 1$ states)

$$\dot{\mathbf{y}}^{(c)} = \tilde{\mathbf{A}}^{(c)}\mathbf{y}^{(c)} - \mathbf{b} + \tilde{\mathbf{B}}^{(c)}\boldsymbol{\xi}^{(c)}$$

Furthermore, it can be shown [59] that $\tilde{\mathbf{A}}^{(c)}$ is a strictly stable matrix (all its eigenvalues are also eigenvalues of $\mathbf{A}^{(c)}$ except its zero eigenvalue, and so have a strictly negative real part), and $\tilde{\mathbf{D}}^{(c)} = \tilde{\mathbf{B}}^{(c)}\tilde{\mathbf{B}}^{(c)\top}$ is positive definite (so all its eigenvalues are real and strictly positive). Assuming that all channels can be classified as either "rapid" or "slow" (this assumption can be relaxed, so that this timescale separation can occur also within a single ion channel as we do in the coupled HHS model - see Fig. F.2A), we concatenate all vectors related to rapid channels $\mathbf{r} \triangleq \left(\mathbf{y}_{(1)}^{\top},...,\mathbf{y}_{(R)}^{\top}\right)^{\top}$ and to slow channels $\mathbf{s} \triangleq \left(\mathbf{y}_{(R+1)}^{\top},...,\mathbf{y}_{(R+S)}^{\top}\right)^{\top}$, where $R+S=C$. We obtain Eqs. 1.12-1.13 by similarly defining $\mathbf{b}$,$\mathbf{b}'$,$\boldsymbol{\xi}$ and $\boldsymbol{\xi}'$ together with the block matrices

$$\mathbf{A}' \triangleq \begin{pmatrix} \tilde{\boldsymbol{A}}^{(1)} & 0 & \dots & 0 \\ 0 & \tilde{\boldsymbol{A}}^{(2)} & \dots & 0 \\ \vdots & \vdots & \ddots & \vdots \\ 0 & 0 & \cdots & \tilde{\boldsymbol{A}}^{(R)} \end{pmatrix}, \ \mathbf{A} \triangleq \begin{pmatrix} \tilde{\boldsymbol{A}}^{(R+1)} & 0 & \dots & 0 \\ 0 & \tilde{\boldsymbol{A}}^{(R+2)} & \dots & 0 \\ \vdots & \vdots & \ddots & \vdots \\ 0 & 0 & \cdots & \tilde{\boldsymbol{A}}^{(R+S)} \end{pmatrix}$$

and similarly for $\mathbf{B}'$ and $\mathbf{B}$. Note that $\mathbf{A}'$ is square with $M' = \sum_{c=1}^{R} K^{(c)} - R$ rows while $\mathbf{A}$ is square with $M = \sum_{c=R+1}^{R+S} K^{(c)} - S$ rows.

C Details of numerical simulations

In all the numerical simulations of the full stochastic CBM we used the SDE Eqs. 1.11-1.13 (MATLAB code will later become available). We used first order Euler–Maruyama integration with a time step of $dt = 5\,\mu$sec (quantitative results were verified also at $dt = 0.5\,\mu$sec). Each stimulation pulse was given as a square pulse with a width of $t_0 = 0.5$ ms and amplitude I_0. The results are not affected qualitatively by our choice of a square pulse shape. We define an AP to have occurred if, after the stimulation pulse was given, the measured voltage has crossed some threshold V_{th} (we use $V_{\text{th}} = -10$ mV in all cases). In all cases where direct stimulation is given, unless stated otherwise , we use periodic stimulation with $I_0 = 7.9\mu$A and $T_* = 50\,$msec. Note that no APs are spontaneously generated.

C.1 Calculation of $p_{\text{AP}}(\mathbf{s})$

We numerically calculated $p_{\text{AP}}(\mathbf{s})$ from a stochastic CBM by setting $\epsilon = 0$ and disabling all the slow kinetics in the model (so we only use Eqs. 1.11 and 1.12). Then, for every value of $\mathbf{s}$ we simulated this "semi-frozen" model numerically by first allowing $\mathbf{r}$ to relax to a steady state and then giving a stimulation pulse with amplitude I_0. We repeat this procedures 200 times for each $\mathbf{s}$, and calculate $p_{\text{AP}}(\mathbf{s})$ as the fraction of simulations that produced an AP. A few comments are in order: (1) In some cases (e.g., the HHMS model) we can use a shortcut and calculate $p_{\text{AP}}(\mathbf{s})$ based on previous results. For example, suppose we know the probability function $\tilde{p}_{\text{AP}}(s)$ for some model with a scalar s and we make the substitution $s = \phi(\mathbf{s})$ where the components of $\mathbf{s}$ represent independent and uncoupled channel types ([46]) - then $p_{\text{AP}}(\mathbf{s}) = \tilde{p}_{\text{AP}}(\phi(\mathbf{s}))$ in the new model. (2) The timescale separation assumption $\tau_{\text{AP}} \ll T_m \ll \tau_{\mathbf{s}}$ implies that all the properties of the generated AP (amplitude, latency etc.) maintain similar causality relations with $\mathbf{s}_m$ as does Y_m, so we can find their distribution using the same simulation we used to find $p_{\text{AP}}(\mathbf{s})$, similarly to the approach taken to compute $L(\mathbf{s})$in the deterministic setting ([60]). (3) Numerical results (Fig. C.1) suggest that we can generally write

$$p_{\text{AP}}(\mathbf{s}) \;=\; \Phi\left(E(\mathbf{s})/\sqrt{N_{\mathbf{r}}}\right) \tag{C.1}$$

where Φ is the cumulative distribution function of the normal distribution, $E(\mathbf{s})$ is some "excitability function" (as defined in [60], so $p_{\text{AP}}(\mathbf{s}) = 0.5$ on the threshold $\Theta = \{\mathbf{s}|E(\mathbf{s}) = 0\}$), and $N_{\mathbf{r}}^{-1/2}$, the "noisiness" of the rapid sub-system, directly affects the slope of $p_{\text{AP}}(\mathbf{s})$ (Fig. C.1D, *bottom*). Also, as explained in [60], $E(\mathbf{s})$ is usually monotonic in each component separately and increasing in I_0 (Fig. C.1C, *top*) - which could be considered as just another component of $\mathbf{s}$ which has zero rates. Note that the I_0 dependency of $p_{\text{AP}}(\mathbf{s})$ is commonly measured experimentally (averaged on the values of $\mathbf{s}$ in the experiment), so this can be used to get a crude lower bound on $N_{\mathbf{r}}$.

Eq. C.1 can be explained heuristically. Recall that the fast variables $(V(t), \mathbf{r}(t))$ follow stereotypically either the "AP response" ($Y_m = 1$) or the "no-AP response" ($Y_m = 0$), then equilibrate rapidly to some quasi-stationary distribution $q(V, \mathbf{r}|\mathbf{s})$, which becomes $q(V, \mathbf{r})$ given assumption 3. Since the voltage response is stereotypical given Y_m, the rapid ion

channels are effectively independent during the response. Also, unless the channel numbers are very low ($N \lesssim 10^2$), the white noise $\boldsymbol{\xi}'$ in Eq. 1.12 can be safely approximated as Gaussian ([24, 46]). Finally, at the rest voltage (V_{rest}), both V and $\mathbf{r}$ display only small fluctuations. Combining all the above facts, we can approximate $\mathbf{r} = \mathbf{r}_* + \hat{\mathbf{r}}$ and $V = V_{\text{rest}} + \mathbf{c}_1^\top \hat{\mathbf{r}}$ where $\hat{\mathbf{r}}$ is a "small" zero mean Gaussian variable and $\mathbf{c}_1$ is some constant vector. Given a sparse spike stimulation, an AP will be generated if and only if $E(V, \mathbf{r}, \mathbf{s}) + X > 0$ where $E(V, \mathbf{r}, \mathbf{s})$ is some excitability function and X is some random variable (possibly dependent on $V, \mathbf{r}$ and $\mathbf{s}$). The AP condition then becomes

$$\begin{aligned} 0 &< E\left(V_{\text{rest}} + \mathbf{c}^\top \hat{\mathbf{r}}, \mathbf{r}_* + \hat{\mathbf{r}}, \mathbf{s}\right) + X \\ &\approx E(V_{\text{rest}}, \mathbf{r}_*, \mathbf{s}) + \mathbf{c}_2^\top \hat{\mathbf{r}} + X \end{aligned}$$

If $\text{Var}\left(\mathbf{c}_2^\top \hat{\mathbf{r}}\right) \gg \text{Var}(X)$ then we get C.1 since $\mathbf{c}_2^\top \hat{\mathbf{r}}$ is a Gaussian variable as a sum of Gaussian variables, with $\text{Var}\left(\mathbf{c}_2^\top \hat{\mathbf{r}}\right) \propto N_{\mathbf{r}}^{-1/2}$ as in (Fig. C.1D, *bottom*).

D Initial condition far from steady state

Transients What happens when the input intervals T_m constitute a WSS process (as in section 2.2), but $\mathbf{s}_m$ is initialized at a value which is far from the steady state? Suppose that this is the case, and that in addition, all our assumptions hold (except for assumption 2). As demonstrated numerically (Fig C.1), and hinted experimentally ([66] Fig. 1A&B), it is common for $p_{\text{AP}}(\mathbf{s})$ to be practically equal to 0 or 1 for most values of $\mathbf{s}$ - except in a small region. Therefore, if we denote $E_+ = \{\mathbf{s} | p(\mathbf{s}) = 1\}, E_- = \{\mathbf{s} | p(\mathbf{s}) = 0\}, E_0 = \{\mathbf{s} | p(\mathbf{s}) \neq 0, 1\}$, then as long as $\mathbf{s}_m$ is not in E_0, we obtain

$$\langle \mathbf{s}_{m+1} - \mathbf{s}_m \rangle = \begin{cases} \left(\left(\mathbf{A}_+ - \mathbf{A}_0\right)\tau_{\mathbf{r}} + T_* \mathbf{A}_0\right)\left(\langle \mathbf{s}_m \rangle - \mathbf{s}_\infty^+\right) & \text{, if } \langle \mathbf{s}_m \rangle \in E_+ \\ \left(\left(\mathbf{A}_- - \mathbf{A}_0\right)\tau_{\mathbf{r}} + T_* \mathbf{A}_0\right)\left(\langle \mathbf{s}_m \rangle - \mathbf{s}_\infty^-\right) & \text{, if } \langle \mathbf{s}_m \rangle \in E_- \end{cases}, \tag{D.1}$$

with $\langle \mathbf{s}_m \rangle \to \mathbf{s}_\infty^\pm = \left(\left(\mathbf{A}_\pm - \mathbf{A}_0\right)\tau_{\mathbf{r}} + T_* \mathbf{A}_0\right)^{-1}\left(\left(\mathbf{b}_\pm - \mathbf{b}_0\right)\tau_{\mathbf{r}} + T_* \mathbf{b}_0\right)$ in each case (since $\left(\mathbf{A}_\pm - \mathbf{A}_0\right)\tau_{\mathbf{r}} + T_* \mathbf{A}_0$ are contracting matrices).

Steady state Eventually $\mathbf{s}_m$ reaches some stable steady state behavior. There are several different possible steady state modes, depending on $\mathbf{s}_\infty^\pm$ (which are affected by I_0 and T_*). If both $\mathbf{s}_\infty^\pm \notin E_0$ then steady state behavior can be found by the following self-consistency arguments (similar to those used in [60]).

1. Responsive: If $\mathbf{s}_\infty^+ \in E_+$, $\mathbf{s}_\infty^- \in E_+$ then $\mathbf{s}_m$ stabilizes at $\mathbf{s}_\infty^+$, so $Y_m = 1$ for all m.
2. Unresponsive: If $\mathbf{s}_\infty^+ \in E_-$, $\mathbf{s}_\infty^- \in E_-$ then $\mathbf{s}_m$ stabilizes at $\mathbf{s}_\infty^-$, so $Y_m = 0$ for all m.
3. Intermittent: If $\mathbf{s}_\infty^- \in E_+$, $\mathbf{s}_\infty^+ \in E_-$ then $\mathbf{s}_m$ stabilizes on a fixed point in E_0, or on an attractor (e.g limit cycle) intersecting E_0.
4. Bi-stable: If $\mathbf{s}_\infty^+ \in E_+$, $\mathbf{s}_\infty^- \in E_-$ then, depending on the initial conditions, $\mathbf{s}_m$ might stabilize either on $\mathbf{s}_\infty^+$ (and then $Y_m = 1$ for all m), on $\mathbf{s}_\infty^-$ (and then $Y_m = 0$ for all m), or (in more pathological cases) on some attractor that intersects E_0.

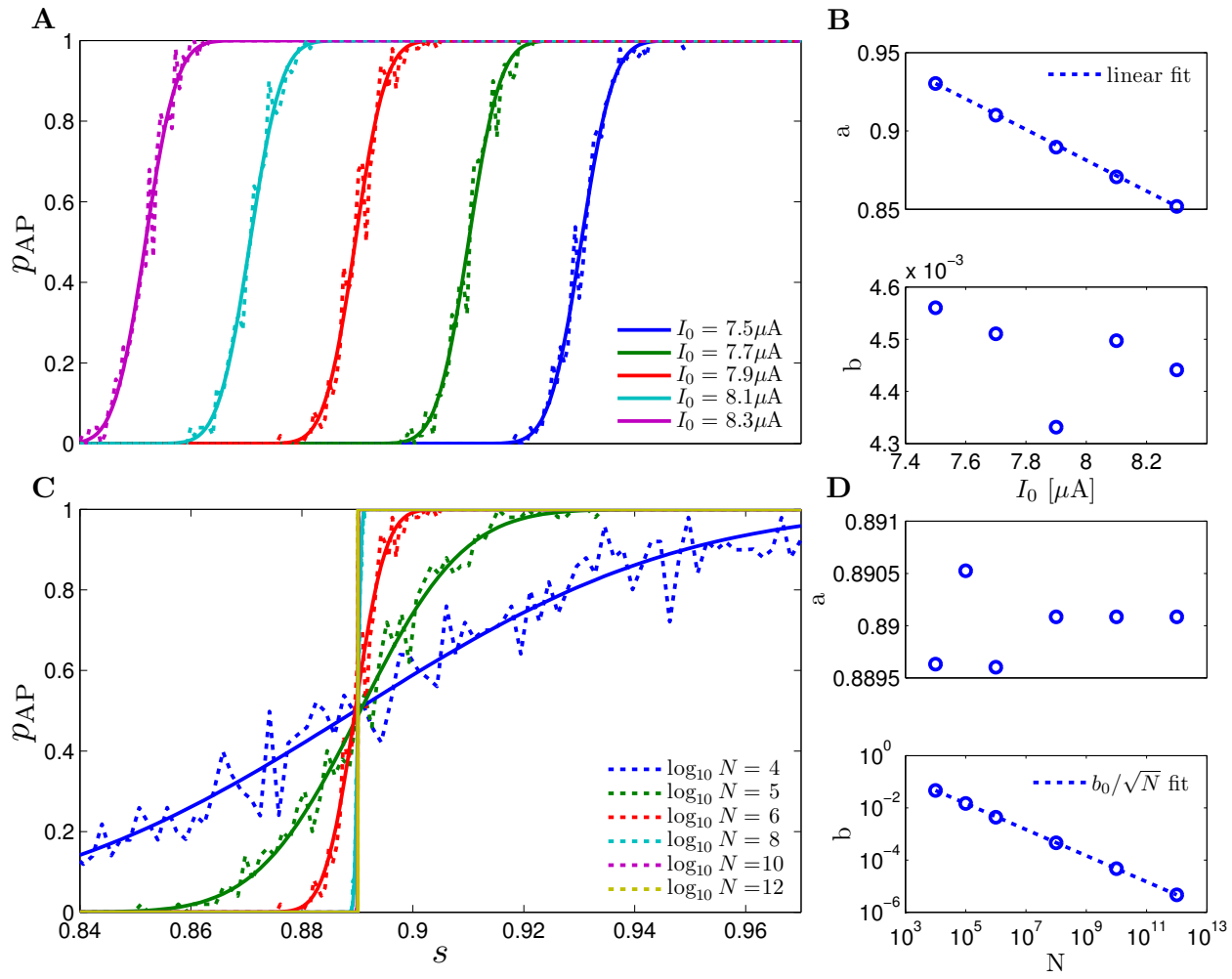

Figure C.1: **Fitting of $p_{\mathrm{AP}}(s) = \Phi((s-a)/b)$ in the stochastic HHS model.** **A** Fitting of $p_{\mathrm{AP}}(s)$ for various values of I_0. **B** Fitting shows that a is linearly decreasing in I_0. **C** Fitting of $p_{\mathrm{AP}}(s)$ for various values of N. **D** Fitting shows that $b \propto 1/\sqrt{N}$.

And so, the steady state neuronal response $\{Y_m\}$ can be a non-constant series only in the intermittent mode, if $\mathbf{s}_\infty^+ \in E_0$, if $\mathbf{s}_\infty^- \in E_0$ or in some bi-stable cases (note that the bi-stable case was not observed in cortical neurons [60]). In these cases, $\{Y_m\}$ becomes a true "stochastic" process, which is coupled with $\{\mathbf{s}_m\}$. Note also, that in both the responsive and unresponsive modes $\mathbf{s}_m$ remains near a stable fixed point. Therefore, if we change stimulation parameters continuously (e.g., T_* or I_0) and reach the intermittent mode at some critical parameter, then the fixed point is still stable (or marginally stable).

E Model Details and Parameters

As argued in the introductory section, a main asset of the present approach is its applicability to a broad range of models of various degrees of complexity and realism. In this section we describe several models and show how they are encapsulated within our general formalism in Figs. 2.1,F.1 and F.2. These models have either been studied in the literature or are extensions of such models, which are meant to explore the limit for the validity of our analytic approximations. In all cases where direct stimulation is given, unless stated otherwise, we use periodic stimulation with $I_0 = 7.9\mu$A and $T_* = 50\,$msec.

The HHS model

The HHS model combines the Hodgkin-Huxley equations ([26]) with slow sodium inactivation ([6, 17]). The model equations ([60]), which employ the uncoupled stochastic noise approximation, are

$$\begin{aligned}
C\dot{V} &= \bar{g}_{Na} s m^3 h \left(E_{Na} - V\right) + \bar{g}_K n^4 \left(E_K - V\right) + \bar{g}_L \left(E_L - V\right) + I\left(t\right) \\
\dot{m} &= \phi\left[\alpha_m\left(V\right)\left(1-m\right) - \beta_m\left(V\right) m\right] + \sqrt{N_h^{-1}\left(\alpha_h\left(V\right)\left(V\right)\left(1-h\right) + \beta_h\left(V\right) h\right)}\xi_m \\
\dot{n} &= \phi\left[\alpha_n\left(V\right)\left(1-n\right) - \beta_n\left(V\right) n\right] + \sqrt{N_h^{-1}\left(\alpha_h\left(V\right)\left(V\right)\left(1-h\right) + \beta_h\left(V\right) h\right)}\xi_n \\
\dot{h} &= \phi\left[\alpha_h\left(V\right)\left(1-h\right) - \beta_h\left(V\right) h\right] + \sqrt{N_h^{-1}\left(\alpha_h\left(V\right)\left(V\right)\left(1-h\right) + \beta_h\left(V\right) h\right)}\xi_h \\
\dot{s} &= \delta\left(V\right)\left(1-s\right) - \gamma\left(V\right) s + \sqrt{N_s^{-1}\left(\delta\left(V\right)\left(1-s\right) + \gamma\left(V\right) s\right)}\xi_s
\end{aligned}$$

Most of the parameters are given their original values (as in [26, 17]):

$$\begin{gathered}
V_{Na} = 50\text{ mV}, \qquad V_K = -77\text{ mV}, \qquad V_L = -54\text{ mV}, \\
\bar{g}_{Na} = 120\ (k\Omega\cdot cm^2)^{-1}, \quad \bar{g}_K = 36\ (k\Omega\cdot cm^2)^{-1}, \quad g_L = 0.3\ (k\Omega\cdot cm^2)^{-1},
\end{gathered}$$

$$\begin{aligned}
\alpha_n(V) &= \tfrac{0.01(V+55)}{1-e^{-0.1\cdot(V+55)}}\text{ kHz}, & \beta_n(V) &= 0.125\cdot e^{-(V+65)/80}\text{ kHz}, \\
\alpha_m(V) &= \tfrac{0.1(V+40)}{1-e^{-0.1\cdot(V+40)}}\text{ kHz}, & \beta_m(V) &= 4\cdot e^{-(V+65)/18}\text{ kHz}, \\
\alpha_h(V) &= 0.07\cdot e^{-(V+65)/20}\text{ kHz}, & \beta_h(V) &= \left(e^{-0.1\cdot(V+35)}+1\right)^{-1}\text{ kHz},
\end{aligned}$$

where in all the rate functions V is used in units of mV. In order to obtain the specific spike shape and the latency transients observed in cortical neurons, some of the parameters were

modified to

$$C_m = 0.5\ \mu\text{F/cm}^2 \quad , \quad \phi = 2$$
$$\gamma(V) = 0.51 \cdot (e^{-0.3\cdot(V+17)} + 1)^{-1}\ \text{Hz} \quad , \quad \delta(V) = 0.05e^{-(V+85)/30}\ \text{Hz}$$

Estimates of channel number greatly vary ([60]). For simplicity, we chose $N = N_n = N_h = N_m = N_s$, and unless stated otherwise, we chose, by default $N = 10^6$, as in [60].

The Coupled HHS model

The coupled version of the HHS model has the same parameters as the uncoupled version, and a similar voltage equation

$$C\dot{V} = \bar{g}_{Na} s_0 m_0 h_0 (E_{Na} - V) + \bar{g}_K n_0 (E_K - V) + \bar{g}_L (E_L - V) + I(t)$$

where the variables the n_0 and $s_0 m_0 h_0$ describe the respective fraction of potassium and sodium channels residing in the "open" state. To obtain the coupled model equations, we need to assume something about the structure of the ion channels. The original assumption by Hodgkin and Huxley was that the channel subunits (e.g., m, n and h) are independent. Over the years, it became apparent that this assumption is inaccurate, and the sodium channel kinetics subunits are, in fact, not independent ([64]). However, it is not yet clear how the slow sodium inactivation is coupled to the rapid channel kinetics (e.g., [39, 42]), so we nevertheless used the original naive HH model assumption that the subunits are independent. In that case the potassium channel structure is given by (for brevity, the voltage dependence of the rates is henceforth ignored for this model)

$$n_0 \underset{\beta_n}{\overset{4\alpha_n}{\rightleftharpoons}} n_1 \underset{2\beta_n}{\overset{3\alpha_n}{\rightleftharpoons}} n_2 \underset{3\beta_n}{\overset{2\alpha_n}{\rightleftharpoons}} n_3 \underset{4\beta_n}{\overset{\alpha_n}{\rightleftharpoons}} n_4$$

while for the sodium channel is described by

$$
\boxed{
\begin{array}{ccccccc}
 & 3\alpha_m & & 2\alpha_m & & \alpha_m & \\
s_0m_0h_0 & \rightleftharpoons & s_0m_1h_0 & \rightleftharpoons & s_0m_2h_0 & \rightleftharpoons & s_0m_3h_0 \\
 & \beta_m & & 2\beta_m & & 3\beta_m &
\end{array}
}
$$

$$\alpha_h \uparrow\downarrow \beta_h$$

$$
\boxed{
\begin{array}{ccccccc}
 & 3\alpha_m & & 2\alpha_m & & \alpha_m & \\
s_0m_0h_1 & \rightleftharpoons & s_0m_1h_1 & \rightleftharpoons & s_0m_2h_1 & \rightleftharpoons & s_0m_3h_1 \\
 & \beta_m & & 2\beta_m & & 3\beta_m &
\end{array}
}
$$

$$\delta \uparrow\downarrow \gamma$$

$$
\boxed{
\begin{array}{ccccccc}
 & 3\alpha_m & & 2\alpha_m & & \alpha_m & \\
s_1m_0h_0 & \rightleftharpoons & s_1m_1h_0 & \rightleftharpoons & s_1m_2h_0 & \rightleftharpoons & s_1m_3h_0 \\
 & \beta_m & & 2\beta_m & & 3\beta_m &
\end{array}
}
$$

$$\alpha_h \uparrow\downarrow \beta_h$$

$$
\boxed{
\begin{array}{ccccccc}
 & 3\alpha_m & & 2\alpha_m & & \alpha_m & \\
s_1m_0h_1 & \rightleftharpoons & s_1m_1h_1 & \rightleftharpoons & s_1m_2h_1 & \rightleftharpoons & s_1m_3h_1 \\
 & \beta_m & & 2\beta_m & & 3\beta_m &
\end{array}
}
$$

Here if transition rates are indicated between two boxed regions, it is to be understood that the same rates are used between all corresponding states in boxed regions. The corresponding 32 SDEs are derived using the method described in [46] (or 30 equations if we use the reduction technique described in). In this model we used $I_0 = 8.3\mu$A.

The HHSTM model

In order to investigate the effect of a more "physiological" stimulation, we changed the HHS model and added synapses. We used the popular Tsodyks-Markram model for the effect of a synapse with short-term-depression on the somatic voltage (the model first appeared in [61]and was slightly corrected in [62]). In the model$x$, y and z are the fractions of resources in the recovered, active and inactive states respectively, interacting through the system

$$
\begin{array}{ccccc}
 & & y & & \\
 & \nearrow & & \searrow & \\
x & & \longleftarrow & & z
\end{array}
\quad . \tag{E.1}
$$

Here the $z \to x$ rate is τ_{rec}^{-1}, the $x \to y$ rate is τ_{in}^{-1}, and the $x \to y$ rate is $U_{SE}\delta\left(t - t_{sp}\right)$, where $\delta\left(\cdot\right)$ is the Dirac delta function, and t_{sp} being the pre-synaptic spike arrival time. The post-synaptic current is given by $I_s\left(t\right) = A_{SE}y\left(t\right)$. Additionally, we added noise to the model using the coupled SDE method ([46]), assuming that diagram E.1 with the corresponding rate hint at the underlying Markov kinetic structure, with $N = 10^6$. As in [61] Fig. 1B, we used $\tau_{\text{in}} = 800\,\text{msec}, \tau_{\text{rec}} = 3\,\text{msec}$ and $U_{SE} = 0.67$. Additionally, we set $A_{SE} = 70\,\mu A$ to obtain an AP response in our model.

The HHMS model

The HHMS model consists of many sodium currents, each with different slow kinetic variable. The equations are identical to the HHS model, except $\bar{g}_{Na}s$ is replaced by $\bar{g}_{Na}M^{-1}\sum_{i=1}^{M}s_i$, where

$$\dot{s}_i = \delta_i(V)(1-s_i) - \gamma_i(V)s_i + \sqrt{N_i^{-1}(\delta_i(V)(1-s_i)+\gamma_i(V)s_i)}\xi_i$$

with $\gamma_i(V) = \gamma(V)\epsilon^i$,$\delta_i(V) = \delta(V)\epsilon^i$ and $N_{(i)} = N\epsilon^{ic}$, where $\gamma(V), \delta(V)$ and N are taken from the HHS model. Also, we chose $\epsilon = 0.2, c = 1.5, M = 5$

The Multiplicative HHMS model

The Multiplicative HHMS model is identical to the HHMS model with $c = 1$, except that $\bar{g}_{Na}M^{-1}\sum_{i=1}^{M}s_i$ is replaced with $\bar{g}_{Na}\prod_{i=1}^{M}s_i$.

The HHSIP model

The HHSIP model equations ([60]) are identical to the HHS mode equations, except that s is renamed to s_1 and an Inactivating Potassium current was is to the voltage equation

$$I_{\mathrm{K}} = \bar{g}_M n^4 s_2 (E_K - V) .$$

with $\bar{g}_M = 0.05\bar{g}_K$ and

$$\dot{s}_2 = \delta_2(V)(1-s_2) - \gamma_2(V)s_2 + \sqrt{N_{s_2}^{-1}(\delta(V)(1-s_2)+\gamma(V)s_2)},$$

where $N_{s_2} = N$ and

$$\delta_2(V) = \frac{3.3e^{(V+35)/15}+e^{-(V+35)/20}}{1+e^{-(V+35)/10}}\ \mathrm{Hz},\ \gamma_2(V) = \frac{3.3e^{(V+35)/15}+e^{-(V+35)/20}}{1+e^{(V+35)/10}}\ \mathrm{Hz}.$$

Again, in all the rate functions V is used in mV units.In this model we used $I_0 = 8.3\mu$A and $T_* = 33$ msec.

The HHMSIP model

The HHMSIP model combines HHSIP and HHMS. Its equations are identical to the HHMS model with $c = 2$, except it also contain the I_{K} current from the HHSIP model. In this model we used $I_0 = 8.3\mu$A and $T_* = 33$ msec, unless otherwise specified.

F Additional Figures

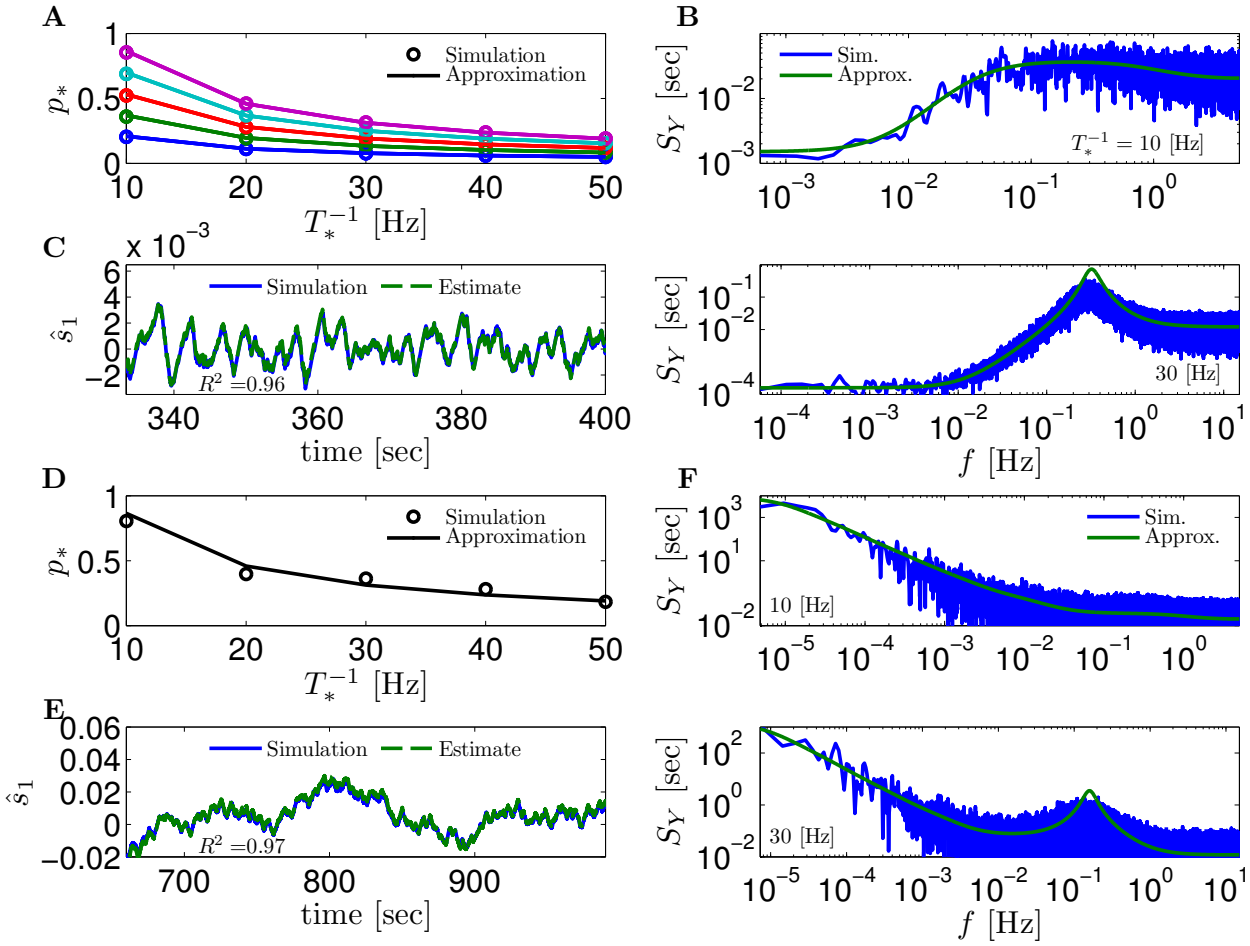

Figure F.1: **Comparing mathematical results with CBM simulation when assumptions break.** In the HHSIP model we plot **A** $p_*\left(T_*^{-1}\right)$ for different currents ($I_0 = 7.5, 7.7, 7.9, 8.1, 8.3$ μA from bottom to top). **B** $S_Y\left(f\right)$ for two values of T_*. Upper figure shows case when $T_* \approx 0.5\tau_{\mathbf{s}}$ so the timescale separation assumption breaks up. In lower figure the parameters are close to a Hopf bifurcation where a limit cycle is formed so the fixed point assumption breaks up, so estimation of limit cycle frequency component is less accurate. **C** Estimation of $\hat{s}_1$ even for $T_*^{-1} \approx 30$ Hz even better than in HHS. Similarly we plot the results of the HHMSIP model in (**D-F**), which has considerable more noise in the slow kinetics, and so even larger fluctuations (which further invalidates the fixed point assumption). See section E for various model details.

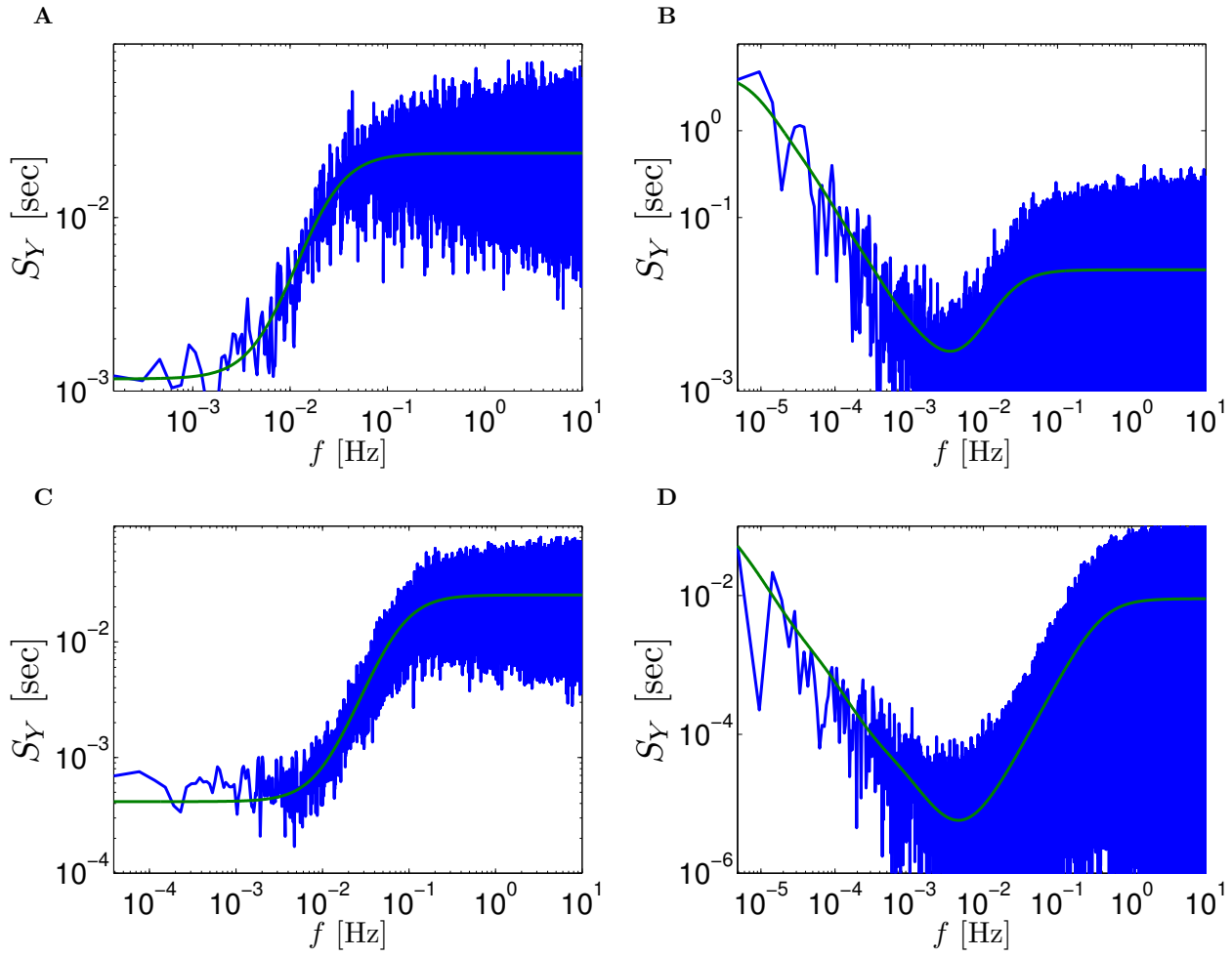

Figure F.2: **Comparing mathematical results (green) with CBM simulation (blue) in various models. A** Coupled HHS **B** HHMS **C** HHSTM **D** Multiplicative HHMS. See section E for various model details.

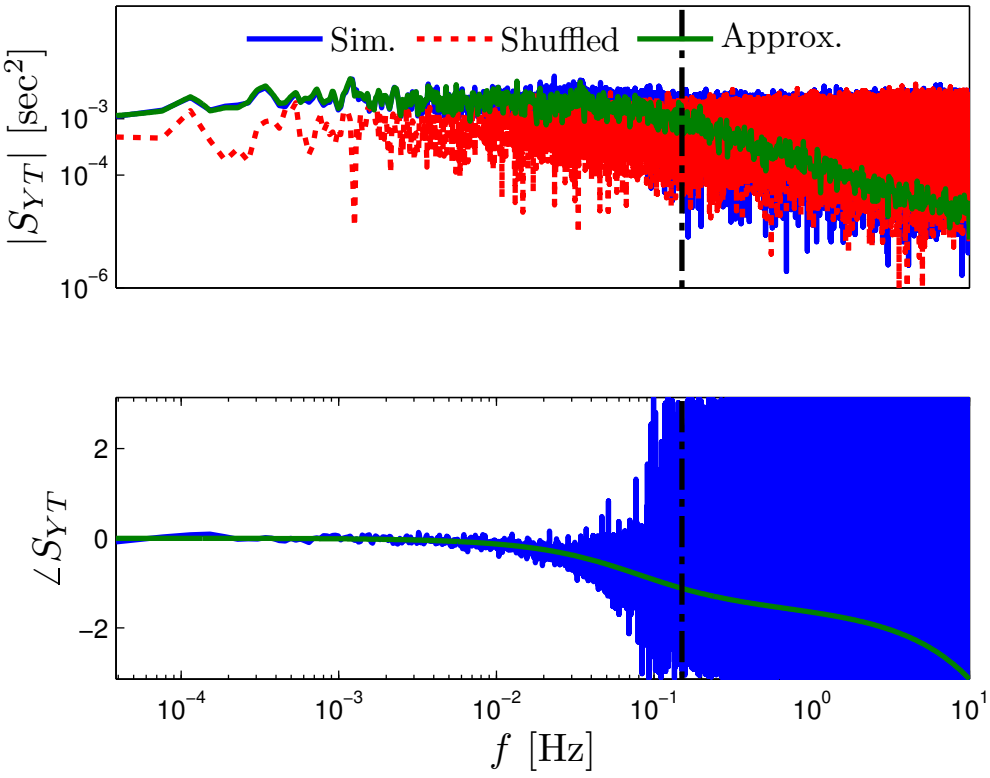

Figure F.3: **Estimation noise in cross-power spectral density.** When estimating cross-spectrum, estimation noise level can be quite high ($\propto$1/coherence, according to [49], p. 321). To estimate the level of this noise in Fig. 2.1D, we added $S_{Y\tilde{T}}(f)$ where $\left\{\tilde{T}_m\right\}$ is a shuffled version of $\{T_m\}$. Only when estimated $S_{YT}(f)$ is above $S_{Y\tilde{T}}(f)$, its estimation is valid. Therefore, in figure 2.1D we show only this region (left of dashed black line), where estimation is valid .

References

[1] B D O Anderson and J B Moore. *Optimal filtering*, volume 11. Dover Publications, Inc., Mineola, New York, 1979.

[2] B P Bean. The action potential in mammalian central neurons. *Nature Reviews Neuroscience*, 8(6):451–65, June 2007.

[3] M Brecht, Miriam Schneider, Bert Sakmann, and Troy W Margrie. Whisker movements evoked by stimulation of single pyramidal cells in rat motor cortex. *Nature*, 427(6976):704–10, February 2004.

[4] Romain Brette and W Gerstner. Adaptive exponential integrate-and-fire model as an effective description of neuronal activity. *Journal of Neurophysiology*, 94(5):3637–42, 2005.

[5] E. N. Brown, Loren M Frank, Dengda Tang, Michael C Quirk, and Matthew A Wilson. A Statistical Paradigm for Neural Spike Train Decoding Applied to. 18(18):7411–7425, 1998.

[6] W K Chandler and H Meves. Slow changes in membrane permeability and long-lasting action potentials in axons perfused with fluoride solutions. *The Journal of Physiology*, 211(3):707, 1970.

[7] D Colquhoun and A G Hawkes. On the Stochastic Properties of Single Ion Channels. *Proceedings of the Royal Society of London. Series B, Biological Sciences (1934-1990)*, 211(1183):205–235, 1981.

[8] Matthew Cook, David Soloveichik, Erik Winfree, and Jehoshua Bruck. Programmability of chemical reaction networks. *Algorithmic Bioprocesses*, 2009.

[9] P Dayan and L F Abbott. *Theoretical neuroscience: Computational and mathematical modeling of neural systems*. MIT Press, 2001.

[10] D Debanne, E Campanac, A Bialowas, and E Carlier. Axon Physiology. *Physiological Reviews*, pages 555– 602, 2011.

[11] Shaul Druckmann, Yoav Banitt, Albert Gidon, Felix Schürmann, Henry Markram, and I Segev. A novel multiple objective optimization framework for constraining conductance-based neuron models by experimental data. *Frontiers in neuroscience*, 1(1):7–18, November 2007.

[12] Shaul Druckmann, Thomas K Berger, Felix Schürmann, Sean Hill, Henry Markram, and I Segev. Effective stimuli for constructing reliable neuron models. *PLoS computational biology*, 7(8):e1002133, August 2011.

[13] B Ermentrout and D. Terman. *Mathematical foundations of neuroscience*, volume 35. Springer Verlag, New York, 2010.

[14] A A Faisal, Luc P J Selen, and Daniel M Wolpert. Noise in the nervous system. *Nature Reviews Neuroscience*, 9(4):292–303, 2008.

[15] Farzad Farkhooi, Eilif Muller, and Martin Nawrot. Adaptation reduces variability of the neuronal population code. *Physical Review E*, 83(5):1–4, May 2011.

[16] R Fitzhugh. Impulses and Physiological States in Theoretical Models of Nerve Membrane. *Biophysical Journal*, 1(6):445–66, July 1961.

[17] I A Fleidervish, A Friedman, and M J Gutnick. Slow inactivation of Na+ current and slow cumulative spike adaptation in mouse and guinea-pig neocortical neurones in slices. *Journal of Physiology*, 493:83–97, 1996.

[18] R Fox and Y Lu. Emergent collective behavior in large numbers of globally coupled independently stochastic ion channels. *Physical Review E*, 49(4):3421–3431, April 1994.

[19] T. Friedlander and N Brenner. Adaptive response by state-dependent inactivation. *Proceedings of the National Academy of Sciences*, 106(52):22558, 2009.

[20] A Gal, D Eytan, A Wallach, M Sandler, J Schiller, and S Marom. Dynamics of Excitability over Extended Timescales in Cultured Cortical Neurons. *Journal of Neuroscience*, 30(48):16332–16342, December 2010.

[21] W Gerstner and W.M. Kistler. *Spiking neuron models: Single neurons, populations, plasticity*. Cambridge Univ Pr, Cambridge, 2002.

[22] W Gerstner and R Naud. Neuroscience. How good are neuron models? *Science (New York, N.Y.)*, 326(5951):379–80, October 2009.

[23] D T Gillespie. The chemical Langevin equation. *The Journal of Chemical Physics*, 113(1):297, 2000.

[24] J.H. Goldwyn, N.S. Imennov, M Famulare, and E Shea-Brown. Stochastic differential equation models for ion channel noise in Hodgkin-Huxley neurons. *Physical Review E*, 83(4):041908, April 2011.

[25] B Hille. Ion channels of excitable membranes. Sinauer Associates, Sunderland, MA 01375, 3 edition, 2001.

[26] A L Hodgkin and A F Huxley. A quantitative description of membrane current and its application to conduction and excitation in nerve. *The Journal of physiology*, 117(4):500, 1952.

[27] Q J M Huys, M B Ahrens, and L Paninski. Efficient estimation of detailed single-neuron models. *Journal of neurophysiology*, 96(2):872, August 2006.

[28] E M Izhikevich. Which model to use for cortical spiking neurons? *IEEE transactions on neural networks*, 15(5):1063–1070, 2004.

[29] E M Izhikevich. *Dynamical systems in neuroscience*. MIT Press, MA, Cambridge, 2007.

[30] C Koch. *Biophysics of computation: information processing in single neurons*. Oxford University Press, New York, 2005.

[31] C Koch and I Segev. *Methods in Neuronal Modeling: From Ions to Networks*, volume 484. MIT press, Cambridge, 2nd edition, 1989.

[32] L Lapicque. Recherches quantitatives sur l'excitation électrique des nerfs traitée comme une polarisation. *Physiol. Pathol. Gen*, 9:620–635, 1907.

[33] L Lennart. System identification: theory for the user. *PTR Prentice Hall, Upper Saddle River, NJ*, 1999.

[34] Yonatan Loewenstein, Annerose Kuras, and Simon Rumpel. Multiplicative dynamics underlie the emergence of the log-normal distribution of spine sizes in the neocortex in vivo. *The Journal of neuroscience : the official journal of the Society for Neuroscience*, 31(26):9481–8, June 2011.

[35] Z F Mainen and T J Sejnowski. Influence of dendritic structure on firing pattern in model neocortical neurons. *Nature*, 382(6589):363–6, July 1996.

[36] E Marder and Jean-Marc Goaillard. Variability, compensation and homeostasis in neuron and network function. *Nature Reviews Neuroscience*, 7(7):563–74, July 2006.

[37] S Marom. Neural timescales or lack thereof. *Progress in Neurobiology*, 90(1):16–28, 2010.

[38] Julian P Meeks and Steven Mennerick. Action potential initiation and propagation in CA3 pyramidal axons. *Journal of Neurophysiology*, 97(5):3460–72, May 2007.

[39] Vilas Menon, Nelson Spruston, and William L Kath. A state-mutating genetic algorithm to design ion-channel models. *Proceedings of the National Academy of Sciences*, 106(39):16829–34, September 2009.

[40] Skander Mensi, Richard Naud, Christian Pozzorini, Michael Avermann, Carl C H Petersen, and Wulfram Gerstner. Parameter Extraction and Classification of Three Cortical Neuron Types Reveals Two Distinct Adaptation Mechanisms. *Journal of neurophysiology*, pages 1756–1775, December 2011.

[41] M Migliore, C Cannia, W W Lytton, Henry Markram, and M L Hines. Parallel network simulations with NEURON. *Journal of computational neuroscience*, 21(2):119–29, October 2006.

[42] Lorin S Milescu, Tadashi Yamanishi, Krzysztof Ptak, and Jeffrey C Smith. Kinetic properties and functional dynamics of sodium channels during repetitive spiking in a slow pacemaker neuron. *The Journal of neuroscience : the official journal of the Society for Neuroscience*, 30(36):12113–27, September 2010.

[43] JD Murray. *Mathematical biology*. Springer, New York, third edit edition, 2002.

[44] Björn Naundorf, Fred Wolf, and Maxim Volgushev. Unique features of action potential initiation in cortical neurons. *Nature*, 440(7087):1060–3, April 2006.

[45] E Neher and B Sakmann. Single-channel currents recorded from membrane of denervated frog muscle fibres. *Nature*, pages 799–802, 1976.

[46] P Orio and D Soudry. Simple, fast and accurate implementation of the diffusion approximation algorithm for stochastic ion channels with multiple states. *PLOS One*, 2012.

[47] L Paninski. Maximum likelihood estimation of cascade point-process neural encoding models. *Network: Computation in Neural Systems*, 15(4):243–262, November 2004.

[48] A. Papoulis and S.U. Pillai. *Probability, random variables, and stochastic processes*. McGraw-Hill New York, 1965.

[49] J S Bendat Piersol and A G. Random Data Analysis and Measurement Procedures. *Measurement Science and Technology*, 11(12):1825–1826, December 2000.

[50] M Pospischil, M Toledo-Rodriguez, C Monier, Z Piwkowska, T Bal, Y Frégnac, H Markram, and A Destexhe. Minimal Hodgkin-Huxley type models for different classes of cortical and thalamic neurons. *Biological Cybernetics*, 99(4-5):427–41, November 2008.

[51] Steven a Prescott and T J Sejnowski. Spike-rate coding and spike-time coding are affected oppositely by different adaptation mechanisms. *The Journal of Neuroscience*, 28(50):13649–61, December 2008.

[52] LR Rabiner. A tutorial on hidden Markov models and selected applications in speech recognition. *Proceedings of the IEEE*, 1989.

[53] A Roth and M Häusser. Compartmental models of rat cerebellar Purkinje cells based on simultaneous somatic and dendritic patch-clamp recordings. *The Journal of physiology*, 535(Pt 2):445–72, September 2001.

[54] David J Schulz, Jean-Marc Goaillard, and E Marder. Quantitative expression profiling of identified neurons reveals cell-specific constraints on highly variable levels of gene expression. *Proceedings of the National Academy of Sciences of the United States of America*, 104(32):13187–91, August 2007.

[55] T Schwalger, K Fisch, J Benda, and B Lindner. How Noisy Adaptation of Neurons Shapes Interspike Interval Histograms and Correlations. *PLoS Computational Biology*, 6(12):e1001026, December 2010.

[56] I Segev and M London. Untangling Dendrites with Quantitative Models. *Science*, 290(5492):744–750, October 2000.

[57] RA Silver. Neuronal arithmetic. *Nature Reviews Neuroscience*, 11(July):474–489, June 2010.

[58] P J Sjostrom, EA Rancz, A Roth, and M Häusser. Dendritic excitability and synaptic plasticity. *Physiological*, 88:769 – 840, 2008.

[59] D Soudry and R Meir. An exact reduction of the master equation to a strictly stable system with an explicit expression for the stationary distribution. *ArXiv*, 2012.

[60] D Soudry and R Meir. Conductance-based neuron models and the slow dynamics of neuronal excitability. *Front. Comput. Neurosci.*, 2012.

[61] M Tsodyks and H Markram. The neural code between neocortical pyramidal neurons depends on neurotransmitter release probability. *Proceedings of the National Academy of Sciences*, 94(2):719–23, January 1997.

[62] M Tsodyks, K Pawelzik, and H Markram. Neural networks with dynamic synapses. *Neural computation*, 10(4):821–35, May 1998.

[63] A.M. Turing. The chemical basis of morphogenesis. *Philosophical Transactions of the Royal Society of London. Series B, Biological Sciences*, 237(641):37, 1952.

[64] Werner Ulbricht. Sodium channel inactivation: molecular determinants and modulation. *Physiological Reviews*, 85(4):1271–301, 2005.

[65] G Wainrib, Michèle Thieullen, and Khashayar Pakdaman. Reduction of stochastic conductance-based neuron models with time-scales separation. *Journal of computational neuroscience*, August 2011.

[66] A Wallach, D Eytan, A Gal, C Zrenner, and S Marom. Neuronal Response Clamp. *Frontiers in Neuroengineering*, 4(April):1–10, 2011.